ORIGINAL ARTICLE



Targeting histone deacetylase suppresses tumor growth through eliciting METTL14-modified m⁶A RNA methylation in ocular melanoma

Ai Zhuang 1,2 \bigcirc | Xiang Gu 1,2 | Tongxin Ge 1,2 | Shaoyun Wang 1,2 | Shengfang Ge 1,2 | Peiwei Chai 1,2 \bigcirc | Renbing Jia 1,2 \bigcirc | Xiangun Fan 1,2 \bigcirc

Correspondence

Xianqun Fan, Renbing Jia and Peiwei Chai, Department of Ophthalmology, Shanghai Ninth People's Hospital, Shanghai JiaoTong University School of Medicine, Shanghai, 200011, P. R. China Email: fanxq@sjtu.edu.cn, renbingjia@sjtu.edu.cn and chaipeiwei123@sjtu.edu.cn

Funding information

Innovative Research Team of High-level Local Universities in Shanghai, Grant/Award Numbers: SHSMU-ZDCX20210900, SHSMU-ZDCX20210902; National Natural

Abstract

Background: Diversified histone deacetylation inhibitors (HDACis) have demonstrated encouraging outcomes in multiple malignancies. N6-methyladenine (m^6A) is the most prevalent messenger RNA modification that plays an essential role in the regulation of tumorigenesis. Howbeit, an in-depth understanding of the crosstalk between histone acetylation and m^6A RNA modifications remains enigmatic. This study aimed to explore the role of histone acetylation and m^6A modifications in the regulation of tumorigenesis of ocular melanoma.

Methods: Histone modification inhibitor screening was used to explore the effects of HDACis on ocular melanoma cells. Dot blot assay was used to detect the global m⁶A RNA modification level. Multi-omics assays, including

Abbreviations: ALKBH5, AlkB homolog 5 RNA demethylase; BRAF, b-raf proto-oncogene; CCK-8, Cell Counting Kit-8; ChIP, chromatin immunoprecipitation; CRYBG3, crystallin beta-gamma domain containing 3; CUT&Tag, Cleavage Under Targets and Tagmentation; DAPI, 4',6-diamidino-2-phenylindole; DOT1L, disruptor of telomeric silencing-1-like; EMT, epithelial-mesenchymal transition; FAT4, FAT tumor suppressor homolog 4; FBS, fetal bovine serum; FTO, fat mass and obesity-associated protein; GAPDH, glyceraldehyde-3-phosphate dehydrogenase; GEPIA, GeneExpression Profiling Interactive Analysis; HDACs, histone deacetylases; HDACis, histone deacetylation inhibitors; HINT2, histidine triad nucleotide binding protein 2; HRP, horseradish peroxidase; H3K27Ac, acetylation of histone 3 at lysine 27; H3K9Ac, acetylation of histone 3 at lysine 9; H3K79, histone H3 lysine 79; IC₅₀, half-maximal inhibitory concentration; IF, immunofluorescence; m⁶A, N6-methyladenine; meRIP-seq, methylated RNA immunoprecipitation sequencing; METTL14, methyltransferase-like 14; METTL3, methyltransferase-like 3; miCLIP-seq, m⁶A individual-nucleotide-resolution cross-linking and immunoprecipitation sequencing; PBS, phosphate buffer solution; PD-1, programmed cell death 1; PP1, protein phosphatase 1; PI3K, phosphoinositide-3 kinase; qPCR, quantitative real-time polymerase chain reaction; RIP, RNA-binding protein immunoprecipitation; SD, standard deviation; SEM, standard error of mean; SEMA3D, Semaphorin 3D; siRNA, small-interfering RNA; shRNAs, short hairpin RNAs; TBST, triethanolamine-buffered saline-tween; TCGA, The Cancer Genome Atlas; WTAP, Wilms tumor 1-associating protein; YTHDF1, YTH N6-methyladenosine RNA binding protein 2; YTHDF3, YTH N6-methyladenosine RNA binding protein 3.

Ai Zhuang, Xiang Gu and Tongxin Ge contributed equally to this work.

This is an open access article under the terms of the Creative Commons Attribution-NonCommercial-NoDerivs License, which permits use and distribution in any medium, provided the original work is properly cited, the use is non-commercial and no modifications or adaptations are made.

© 2023 The Authors. Cancer Communications published by John Wiley & Sons Australia, Ltd. on behalf of Sun Yat-sen University Cancer Center.

¹Department of Ophthalmology, Shanghai Ninth People's Hospital, Shanghai JiaoTong University School of Medicine, Shanghai, P. R. China ²Shanghai Key Laboratory of Orbital Diseases and Ocular Oncology, Shanghai, P. R. China

Science Foundation of China,
Grant/Award Number: 82103240; Science
and Technology Commission of Shanghai
Municipality, Grant/Award Numbers:
20DZ2270800, 23ZR1438400,
23ZR1480100, 23YF1422400;
Cross-disciplinary Research Fund of
Shanghai, Shanghai Jiao Tong University
Ninth People's Hospital, Grant/Award
Numbers: JYJC202210, YG2023QNB15;
Shanghai Key Clinical Specialty, Shanghai
Eye Disease Research Center,
Grant/Award Number: 2022ZZ01003

RNA-sequencing, cleavage under targets and tagmentation, single-cell sequencing, methylated RNA immunoprecipitation-sequencing (meRIP-seq), and m⁶A individual nucleotide resolution cross-linking and immunoprecipitation-sequencing (miCLIP-seq), were performed to reveal the mechanisms of HDACis on methyltransferase-like 14 (*METTL14*) and FAT tumor suppressor homolog 4 (*FAT4*) in ocular melanoma. Quantitative real-time polymerase chain reaction (qPCR), western blotting, and immunofluorescent staining were applied to detect the expression of *METTL14* and *FAT4* in ocular melanoma cells and tissues. Cell models and orthotopic xenograft models were established to determine the roles of METTL14 and FAT4 in the growth of ocular melanoma. RNA-binding protein immunoprecipitation-qPCR, meRIP-seq, miCLIP-seq, and RNA stability assay were adopted to investigate the mechanism by which m⁶A levels of *FAT4* were affected.

Results: First, we found that ocular melanoma cells presented vulnerability towards HDACis. HDACis triggered the elevation of m⁶A RNA modification in ocular melanoma. Further studies revealed that *METTL14* served as a downstream candidate for HDACis. *METTL14* was silenced by the hypo-histone acetylation status, whereas HDACi restored the normal histone acetylation level of *METTL14*, thereby inducing its expression. Subsequently, METTL14 served as a tumor suppressor by promoting the expression of *FAT4*, a tumor suppressor, in a m⁶A-YTH N6-methyladenosine RNA-binding protein 1-dependent manner. Taken together, we found that HDACi restored the histone acetylation level of *METTL14* and subsequently elicited METTL14-mediated m⁶A modification in tumorigenesis.

Conclusions: These results demonstrate that HDACis exert anti-cancer effects by orchestrating m⁶A modification, which unveiling a "histone-RNA crosstalk" of the HDAC/*METTL14/FAT4* epigenetic cascade in ocular melanoma.

KEYWORDS

epigenetics, histone deacetylation inhibitors, melanoma, N6-methyladenine, histone-RNA crosstalk

1 | BACKGROUND

Histone acetylation is an essential epigenetic marker for gene regulation. Histone acetylation is versatile and highly dynamic, governing transcription, and indispensable in biological processes, including DNA repair, RNA splicing, and stemness maintenance [1]. Moreover, dysregulation of histone acetylation homeostasis contributes to diverse pathogenesis, especially in cancer [2]. For example, nuclear receptor subfamily 4 group A member 1 promoted the acetylation of histone 3 at lysine 27 (H3K27Ac) in the tumor microenvironment, leading to the activation of tolerance-related genes, and thereby inducing T cell dysfunction [3]. Histone acetylation is dynamically erased by histone deacetylases (HDACs), the inhibitors of

which have been widely applied in clinical and pre-clinical stages to treat diverse malignancies, including breast cancer [4], lung cancer [5], and melanoma [6]. For example, HDAC inhibitors (HDACis) were shown to be promising in combination with MEK inhibitors and anti-programmed cell death 1 (PD-1) drugs in advanced uveal melanoma [6, 7]. Taken together, these data indicated that histone modifications play an essential role in the regulation of carcinogenesis.

The N6-methyladenine (m⁶A) RNA modification is the most prevalent messenger RNA modification and plays an essential role in the regulation of RNA metabolism, ranging from RNA processing, nuclear export, and RNA translation to decay [8, 9]. Typically, dynamic m⁶A RNA modifications are catalyzed by methyltransferase-like 3

(METTL3) and METTL14, whereas they are erased by AlkB homolog 5 RNA demethylase (ALKBH5) and fat mass and obesity-associated protein (FTO) [10]. To date, the loss of homeostasis of m⁶A RNA modification was identified as an important trigger for multiple cancers, including leukemia, breast cancer, and melanoma [11, 12]. For example, the loss of the m⁶A-binding protein YTH N6-methyladenosine RNA-binding protein 1 (YTHDF1) activated antigen-specific CD8⁺ T-cell response, making YTHDF1 an anti-cancer target in immunotherapy [13]. In addition, we demonstrated that the downregulation of m⁶A led to translational deficiency of histidine triad nucleotide-binding protein 2 (HINT2), a tumor suppressor in ocular melanoma [14]. These findings indicate that m⁶A RNA modifications are important for carcinogenesis.

Ocular melanomas, including uveal melanoma and conjunctival melanoma, exhibit an aggressive growth pattern, with high rates of metastasis and mortality [15, 16]. Although ocular melanoma is rare, occurring in only 0.5-10 per million people, it is receiving increasing attention [15]. Both uveal melanoma and conjunctival melanoma are sight- and life-threatening malignancies that show distinct patterns of gene expression compared to cutaneous melanoma. However, the effects of most therapies on these genetic deficiencies remain unsatisfactory. Importantly, HDACis demonstrated promising results in the treatment of uveal melanoma [6, 7, 17, 18] and conjunctival melanoma [19] in both clinical trials and pre-clinical models. Intriguingly, decreased m⁶A levels, associated with tumorigenicity, metabolic reprogramming, and response to the anti-PD-1 blockade, served as a prooncogenic factor in melanoma [20–23]. Albeit numerous efforts have been made to explore the role of histone acetylation and m⁶A modifications in the regulation of tumorigenesis [24], a comprehensive understanding of the crosstalk between these two essential modifications is currently lacking. Thus, our study explored the effects of HDACis on ocular melanoma cells and the global m⁶A RNA modification level of ocular melanoma cells. Multi-omics assays were performed to reveal the mechanisms of HDACis on METTL14 and FAT tumor suppressor homolog 4 (FAT4) in ocular melanoma. The expression levels of METTL14 and FAT4 in ocular melanoma cells and tissues were detected. Cell models and orthotopic xenograft models were applied to determine the roles of METTL14 and FAT4 in the growth of ocular melanoma. RNA-binding protein immunoprecipitation-quantitative real-time polymerase chain reaction (RIP-qPCR), methylated RNA immunoprecipitation-sequencing (meRIP-seq), m⁶A individual nucleotide resolution cross-linking and immunoprecipitation-sequencing (miCLIP-seq), and RNA stability assay were adopted to investigate the mechanism by which m⁶A levels of *FAT4* were affected.

2 | METHODS

2.1 | Cell lines and cell culture

Human uveal melanoma cells (MEL290, OMM2.3, and OMM1) and human conjunctival melanoma cells (CRMM1, CRMM2, and CM2005.1) were kindly provided by Professor Martine J. Jager (Leiden University Medical Center, Leiden, Netherlands). The uveal melanoma cell line MUM2B was a gift from Professor John F. Marshall (Centre for Tumor Biology, Cancer Research UK Centre of Excellence, London, UK). The uveal melanoma cell line 92.1, human retinal pigment epithelial cell line ARPE-19 and cutaneous melanoma cell lines (A375 and SK28) were purchased from American Type Culture Collection (Manassas, VA, USA). PIG1, a normal human melanocyte line, was provided by the Department of Ophthalmology, Peking University Third Hospital (Beijing, China). The culture medium used for MUM2B, MEL290, and ARPE-19 cells was Dulbecco's modified Eagle's medium (Gibco, Thermo Fisher Scientific, Waltham, MA, USA). The culture medium used for 92.1, OMM2.3, and OMM1 cells was RPMI-1640 medium (Gibco). Conjunctival melanoma and PIG1 cells were cultured in Ham's F12K medium (Gibco). All culture media were supplemented with 10% fetal bovine serum (FBS, Gibco) and 1% penicillin/streptomycin. The cells were cultured at 37°C in a humidified 5% CO₂ atmosphere. All in vitro cell lines were validated by short tandem repeat profiling and confirmed to be mycoplasma-free.

2.2 | Histone modification inhibitor screening

Histone modification inhibitors used for screening (Supplementary Table S1) were purchased from Selleck (Shanghai, China). CRMM1, 92.1, and PIG1 cells were screened in parallel with the inhibitors at a concentration of 1 μ mol/L in 96-well plates (Corning, Corning, NY, USA). After 24 h, cell viability was measured using a Cell Counting Kit-8 (CCK-8, Dojindo, Shanghai, China). The absorbance of the samples was measured at 450 nm using a microplate reader (Thermo Fisher Scientific). Inhibitors with an inhibitory rate of >60% in ocular melanoma cells and <30% in PIG1 cells were selected. Further evaluation was performed using a 3-fold dilution series of the selected inhibitors. Cell viability was evaluated after 48 h using the CCK-8 assay. The half-maximal inhibitory concentration (IC₅₀) was calculated using the Prism software (version 8.0; GraphPad, San Diego, CA, USA). The selective index towards ocular melanoma cells was calculated as follows: selective index = IC_{50} (average in tumor cells) / IC_{50} (normal

cells) [25, 26]. The selective index > 5 was considered to indicate sufficient selective inhibition efficacy on ocular melanoma.

2.3 | CCK-8 assay

PIG1, uveal melanoma, and conjunctival melanoma cell suspensions were prepared at a concentration of 30,000 cells/mL. The cell suspension (100 μ L/well) was seeded in triplicates in 96-well plates. CCK-8 solution (10 μ L/well) was added for further detection. After incubation at 37°C for 2-4 h, absorbance was measured at 450 nm. Each independent experiment was performed in triplicate.

2.4 | Colony formation assay

PIG1, uveal melanoma, and conjunctival melanoma cells were seeded at 500 cells/well and cultured in 12-well plates (Corning). After 1-2 weeks of incubation at 37°C, the cells were gently rinsed with phosphate buffer solution (PBS), fixed with methanol, and stained with 1% crystal violet for at least 30 min. The excess dye was then rinsed and dried in the air, and colonies were scanned by a flatbed scanner (Hewlett-Packard, Palo Alto, CA, USA) and counted by ImageJ software (version 1.8.0, National Institutes of Health, Bethesda, MD, USA).

2.5 | Transwell assay

A 24-well transwell system with 8- μ m pore size polycarbonate filters (Corning) was used to detect the migration ability of uveal melanoma and conjunctival melanoma cells. To the upper chamber, 1.0×10^4 - 1.0×10^5 tumor cells suspended in 200-250 μ L culture medium with 2% FBS were added, while the lower chambers were filled with 600-650 μ L culture medium with 10% FBS. After incubation at 37°C for 24 h, cells were fixed with methanol and stained with 1% crystal violet (C8470, Amresco, San Diego, CA, USA). The cells in the upper chambers were removed, and those that migrated to the lower chambers were photographed by ECLIPSE Ti inverted microscope system (Nikon Precision, Shanghai, China) and counted by ImageJ software.

2.6 | Orthotopic xenograft assay

Animal experiments were approved by the Shanghai JiaoTong University School of Medicine Animal Ethics Committee (SH9H-2021-A058-SB) and complied with institutional and international guidelines for animal care and

use. Four-week-old BALB/c nude mice were obtained from Slack Company (Shanghai, China) and raised in the specific pathogen-free Laboratory Animal Room of the hospital. After anesthesia with inhaled isoflurane (100150, Yuyan Instruments, Shanghai, China), 2×10^4 92.1 cells in 2 uL sterile PBS were injected into the right vitreous cavity using a microscopic syringe (Hamilton, Reno, NV, USA). The eyes were treated with erythromycin eye ointment. Bioluminescence was detected using in vivo IVIS spectrum imaging systems (PerkinElmer, Waltham, MA, USA) 14 days after injection. All mice were subjected to cervical dislocation 30 days after implantation. Humanitarian euthanasia should be carried out in advance when intraocular tumors cause absolute glaucoma with severe eye pain, or the mice are in poor general condition such as rapid weight loss of more than 15%.

2.7 | Western blotting assay

Western blotting was performed as previously described [14]. Briefly, the polyvinylidene fluoride membranes (Merck-Millipore, Shanghai, China) with the transferred proteins were first incubated with a primary antibody overnight at 4°C, and then with a secondary antibody conjugated to a fluorescent tag or a horseradish peroxidase (HRP) tag. The band signals were tested using an Odyssey infrared imaging system (LI-COR, Lincoln, NE, USA) or a chemiluminescence imaging system (Tanon, Shanghai, China). Antibodies against the following antigens were used: acetylation of histone 3 at lysine 9 (H3K9Ac, 1:2,000, AM39038, Active Motif, Tokyo, Japan), H3K27Ac (1:2,000, AM39034, Active Motif), histone 3 (H3, 1:10,000, 17168-1-AP, Proteintech, Shanghai, China), METTL14 (1:1,000, ab220030, abcam, Cambridge, MA, USA), METTL3 (1:1,000, 15073-1-AP, Proteintech), Wilms tumor 1-associating protein (WTAP) (1:1,000, 60188-1-lg, Proteintech), FTO (1:2,000, 27226-1-AP, Proteintech), ALKBH5 (1:5,000, 16837-1-AP, Proteintech), YTHDF1 (1:5,000, 17491-1-AP, Proteintech), YTHDF2 (1:5,000, 24744-1-AP, Proteintech), YTHDF3 (1:2,000, 25537-1-AP, Proteintech), FAT4 (1:1,000, ab130076, Abcam), and glyceraldehyde-3-phosphate dehydrogenase (GAPDH) (1:10,000, 60004-1-lg, Proteintech).

2.8 | Immunohistochemistry (IHC)

Tissue slides embedded in paraffin were dewaxed, rinsed, and heated to 95°C. After repair with cell conditioning solution, the slides were rinsed and reduced to 37°C. The slides were rinsed at 36°C, primary antibody was added and incubated for 16 min. After rinsing, UV RED

UNIV MULT (Roche, Basel, Kanton Basel, Switzerland) was added and incubated with slides for 12 min. UV RED Enhancer (Roche) was added and incubated for 4 min. After rinsing, UV Fast Red A UV Red Naphthol (Roche) was added and incubated for 8 min. After rinsing, UV Fast Red B (Roche) was added and incubated for 8 min. The slide was rinsed, HEMATOXYLIN II (Roche) was added, and incubated for 8 min. After washing, BLUING REAGENT (Roche) was added and incubated for 4 min. IHC scores were computed through multiplying staining intensity grade (0, 1, 2, and 3 represented negative, weakly positive, moderately positive, and strongly positive staining, respectively) by positive rate score (0, 1, 2, 3, and 4 represented positive areas of $\leq 5\%$, 6%-25%, 26%-50%, 51%–75%, and \geq 76%, respectively) [27]. The following primary antibodies were used in this study: METTL14 (1:300, HPA038002, Sigma-Aldrich) and FAT4 (1:300, #C48034, Signalway Antibody, College Park, MD, USA).

2.9 | Immunofluorescence (IF)

Tissues embedded in paraffin were deparaffinized, rehydrated, fixed, and blocked with 5% normal goat serum, and were then incubated with the primary antibody anti-Ki67 (1:400, ab15580, Abcam) at 4°C overnight. Next, the tissue slides were incubated with secondary antibodies for 60 min, and 4',6-diamidino-2-phenylindole (DAPI, Sigma-Aldrich, St. Louis, MO, USA) was used to counterstain nuclei for 5 min. Digital images were acquired using a ZEISS Axio Scope A1 upright microscope (Oberkochen, Baden-Württemberg, Germany).

2.10 | RNA extraction, reverse transcription, and qPCR

Total RNA of ocular melanoma cells and normal cells was extracted using an EZpress RNA purification kit (B0004, EZBioscience, Beijing, China). Reverse transcription was performed using a PrimeScript RT-PCR kit (Takara Biotechnology, Dalian, Liaoning, China). qPCR was performed using a standard SYBR Green PCR kit (Applied Biosystems, Thermo Fisher Scientific) according to the manufacturer's instructions. GAPDH was used as an internal control. The primers used are listed in Supplementary Table S2.

2.11 | RNA m⁶A dot blotting assay

Total RNA was extracted from uveal melanoma cells, conjunctival melanoma cells, cutaneous melanoma cells

and normal cells, and spotted onto nitrocellulose membranes (Merck-Millipore). The membranes were then cross-linked with ultraviolet light and blocked with 5% milk for 1 h. The membranes were incubated with m⁶A antibody (1:1,000, #56593S, Cell Signaling Technology, Boston, MA, USA) overnight at 4°C, washed three times with triethanolamine-buffered saline-tween (TBST), and subsequently incubated with secondary goat anti-rabbit IgG-HRP at room temperature for 1 h. The membranes were then washed with TBST and visualized using an imaging system (Tanon). Another membrane was spotted and stained with 0.02% methylene blue (Sigma-Aldrich) to ensure baseline consistency among the different groups.

2.12 | Tissue specimens

From January 2007 to December 2017, 56 human ocular melanoma samples and 27 healthy human melanocytic nevi samples were collected and pathologically confirmed at the Shanghai Ninth People's Hospital, Shanghai Jiao-Tong University School of Medicine (Shanghai, China). The ethics approval for the use of tissue specimens in this study was obtained from Shanghai Ninth People's Hospital (SH9H-2019-T185-2). The sample list and follow-up information were retrospectively obtained from the inpatient history system and ocular tumor follow-up database. Detailed sample information has been described (Supplementary Tables S3-S5).

2.13 | Small-interfering RNA (siRNA)

CRMM1 and 92.1 cells were seeded in 6-well plates at approximately 300,000 cells per well and transfected with siRNA using Lipofectamine 3000 in Opti-MEM (Gibco). At 6 h later, the medium was replaced with a fresh complete medium. RNA extraction, CCK-8 assay, Transwell assay, and colony formation assay were performed after 48 h, and protein extraction was performed after 72 h. Specific primers for silencing *METTL14*, *FAT4*, *YTHDF1*, *YTHDF2*, and *YTHDF3* are listed in Supplementary Table S2.

2.14 | Plasmid construction, lentiviral packaging, and generation of stable cell lines

To overexpress *METTL14*, a *METTL14* cassette was generated by PCR, inserted into the pGMLV-6751 vector, and verified by DNA sequencing. Short hairpin RNAs



(shRNAs) and verified negative control sequences were generated using PCR and cloned into the pGMLV-SC5 vector.

HEK239T cells were transfected with a mixture of 3 µg plasmid, 3 µg pMD2.D plasmid, and 6 µg PsPax plasmid using Lipofectamine 3000 (Invitrogen, Carlsbad, CA, USA) in Opti-MEM (Gibco). At 6 h later, the medium was replaced with a fresh complete medium. The viruscontaining supernatant was collected 48 and 72 h after transfection, filtered through a 0.45-mm cellulose acetate filter, and concentrated using a Lenti-X Concentrator (Takara). Medium containing 25 μL/mL concentrated lentivirus and 5 ng/mL polybrene (Sigma-Aldrich) was added to cells seeded 24 h before transduction, and the cells were maintained in the virus-containing medium for 48 h. Stable cell lines were selected by incubation with 4 μg/mL puromycin (InvivoGen, Beijing, China) for 2 weeks and maintained in a medium containing $1 \mu g/mL$ puromycin. The primer sequences are listed in Supplementary Table S2.

2.15 | Cleavage Under Targets and Tagmentation (CUT&Tag), library construction, and DNA sequencing

The CUT&Tag assay was performed as previously reported [27]. Briefly, 1×10^5 cells were harvested, washed, and mixed with activated concanavalin A-coated magnetic beads (Bangs Laboratories, Fishers, IN, USA) at room temperature for 15 min. The cells were incubated with primary antibody (1:50) overnight at 4°C, washed thrice, and then incubated with secondary antibody (1:50) at room temperature for approximately 1 h. After washing, the cells were incubated in 100 μ L of pA-Tn5 adapter complex (~40 nmol/L) at room temperature for approximately 1 h. After washing, the cells were resuspended in Tagmentation buffer (50 μ L) and incubated at 37°C for 1 h. DNA was then purified and prepared for PCR. Pooled libraries were purified using 1.1× AMPure XP beads. Paired-end Illumina sequencing was performed using a HiSeq 4000 instrument (Illumina, San Diego, CA, USA). Antibodies against the following antigens were used: H3K9Ac (1:2,000), H3K27Ac (1:2,000).

2.16 | Chromatin immunoprecipitation (ChIP)

ChIP assays were performed as previously described, using an EZ-Magna ChIP A/G kit (Millipore) [28]. Cells (1×10^8) were lysed using cell lysis buffer and nuclear lysis buffer. Cell lysates were sonicated for 10 min (10 s on and 15 s

off) on ice. Antibodies against H3K27Ac, H3K9Ac, and IgG (ab172730, Abcam) were added to diluted chromatin fragments. Protein A/G magnetic beads were applied to each IP and incubated with rotation overnight at 4°C. DNA was then removed from the protein/DNA complexes. Purified DNA fragments were amplified by PCR. The specific primers used for the ChIP-PCR analysis are listed in Supplementary Table S2.

2.17 | RIP-qPCR

The RIP assay was performed using a Magna RIP Quad Kit (Millipore). Briefly, 2.0×10^7 cells were treated with 100 μ L of RIP lysis buffer, of which 10 μ L of supernatant was used as input, and 100 μ L of supernatant was enriched with antibody- or rabbit IgG-conjugated protein A/G magnetic beads in IP buffer supplemented with RNase inhibitors and incubated overnight at 4°C. After washing, the immunoprecipitated RNA was digested, purified, and analyzed by qPCR.

2.18 | meRIP-seq

The meRIP assay was performed using a GenSeq m⁶A meRIP kit (GenSeq, Shanghai, China) [14, 29]. Briefly, total RNA was randomly fragmented using RNA fragmentation buffer and subjected to IP with an anti-m⁶A antibody (ab151230, Abcam) and PGM magnetic beads in IP buffer supplemented with RNase inhibitor. The m⁶A-containing RNA fragments were eluted with MS magnetic beads in RLT buffer and purified using TRI-zol reagent. For the meRIP-seq, two sets of samples were collected for duplicate biological replicates. The samples were sequenced using an Illumina HiSeq 4000 platform (Illumina). Three biological replicates were used for meRIP-qPCR.

2.19 | miCLIP-seq

Small-scale, single-base resolution m⁶A methylome detection was carried out following procedures modified from previous reports [14, 29]. Briefly, 100 ng of mRNA was isolated from cell samples, fragmented to ~100 nucleotides, and incubated with anti-m⁶A antibody in IP buffer under gentle rotation at 4°C for 2 h. The mixture was then irradiated using a CL-1000 ultraviolet crosslinker. After irradiation, the mixture was incubated with pre-washed Dynabeads Protein A (1001D, Life Technologies, Thermo Fisher Scientific) at 4°C for 2 h. After washing, the samples on the beads were subjected to dephosphorylation

with T4 polynucleotide kinase (M0201L, New England Biolabs, Ipswich, MA, USA) at 37°C for 20 min. The RNA was then purified, subjected to library construction using the SMARTer smRNA-Seq Kit (Clontech Laboratories, Shanghai, China) for Illumina according to the manufacturer's instructions, and sequenced using the Illumina HiSeq X Ten platform (Illumina).

2.20 | The Cancer Genome Atlas (TCGA) database

TCGA (http://www.cbioportal.org) and GeneExpression Profiling Interactive Analysis (GEPIA, http://gepia.cancer-pku.cn) were queried to validate the potential roles of *FAT4*, crystallin beta-gamma domain containing 3 (*CRYBG3*), and Semaphorin 3D (*SEMA3D*) in uveal melanoma. The database provides the transcriptional landscape and follow-up information of 78 patients with uveal melanoma.

2.21 | Statistical analysis

GraphPad Prism software (version 8.0) was used for the statistical analyses. Data are presented as mean \pm standard deviation (SD), mean \pm standard error of mean (SEM), or median with interquartile range as required, and an unpaired two-tailed Student's t-test or nonparametric test was used to assess the differences between the two groups. Survival plots were depicted with Kaplan-Meier curves, and P values were calculated with the log-rank test. P value < 0.05 was considered statistically significant. The CancerSEA database (http://biocc.hrbmu.edu. cn/CancerSEA/) was queried to validate that the functional state METTL14 is related to uveal melanoma at single-cell resolution.

3 | RESULTS

3.1 | HDACis exhibited tumor-selective killing efficacy on ocular melanoma

Numerous inhibitors that target posttranslational histone-modifying enzymes have been shown to suppress tumor growth and enhance sensitivity towards chemo-/immunotherapy in ocular melanoma. For example, the inhibitor of disruptor of telomeric silencing-1-like (DOT1L), a methyltransferase of histone H3 lysine 79 (H3K79), epigenetically silenced nicotinate phosphoribosyltransferase (NAPRT) expression through the diminishment of dimethylation of H3K79 in the NAPRT

promoter, thereby inhibiting the malignant behaviors of uveal melanoma [25]. The HDACi JSL-1 increased the expression of tumor suppressor genes, such as p21, p27, and p53, and abrogated the proliferation and metastasis of uveal melanoma cells [30]. The HDAC2 inhibitor santacruzamate A restored the normal acetylation level of PD-L1, blocking its nuclear translocation and thereby attenuating tumor angiogenesis of uveal melanoma [31]. To explore the clinical potential of these epigenetic drugs, we performed high-throughput inhibitor library screening using 245 epi-drugs (Supplementary Table S1). The first-round screening showed that 6 inhibitors, including four HDACis, triggered > 60% inhibitory efficacy in both ocular melanoma cell lines (92.1 and CRMM1) and < 30% in normal melanocytes (Figure 1A-B). Relative cell viability of ocular melanoma cells (92.1 and OMM2.3) compared to normal melanocytes (PIG1) in primary screening and the scatter diagram of cell viability were presented. LBH589 showed selective efficacy in killing ocular melanoma cells (Supplementary Figure S1A-B). In the second round of validation, we compared the IC₅₀ of each inhibitor between ocular melanoma cell lines and normal melanocytes. Three HDACis, LBH589, RG2833, and LMK-235, exhibited tumor-selective inhibition with a selective index > 5 (Figure 1C). Among the 3 HDACis, LBH589 exhibited the highest selective index (> 10) and the lowest IC₅₀ value in ocular melanoma cells (Supplementary Figure S1C). Taken together, these data indicated that LBH589 exhibited high efficacy and low toxicity in treating ocular melanomas.

As LBH589 is an important member of the HDACi family, we tested global histone acetylation levels in ocular melanoma cells after LBH589 treatment. The levels of histone acetylation markers (H3K27Ac and H3K9Ac) were significantly increased in the 3 ocular melanoma cell lines (Figure 1D-E). Notably, 100 nmol/L LBH589 induced a saturated histone acetylation level; therefore, we chose 100 nmol/L as the working concentration of LBH589 in this study. We found that the colony formation capacity of ocular melanoma cells was significantly impaired after 100 nmol/L LBH589 treatment (Figure 1F-G). In addition, ocular melanoma cells exhibited attenuated cellular proliferation (Supplementary Figure S2A) and migration capacity (Supplementary Figure S2B) after LBH589 treatment. In contrast, 100 nmol/L LBH589 did not affect colony formation (Figure 1F-G) and proliferation (Supplementary Figure S2A) of normal melanocytes. To verify the role of LBH589-induced inhibition in vivo, we established an orthotopic ocular melanoma xenograft model by 92.1 cells with a luciferase tag (Figure 1H). Animal imaging showed that LBH589-treated group exhibited decreased bioluminescence intensity and tumor volumes compared to the control group. These findings indicate that LBH589

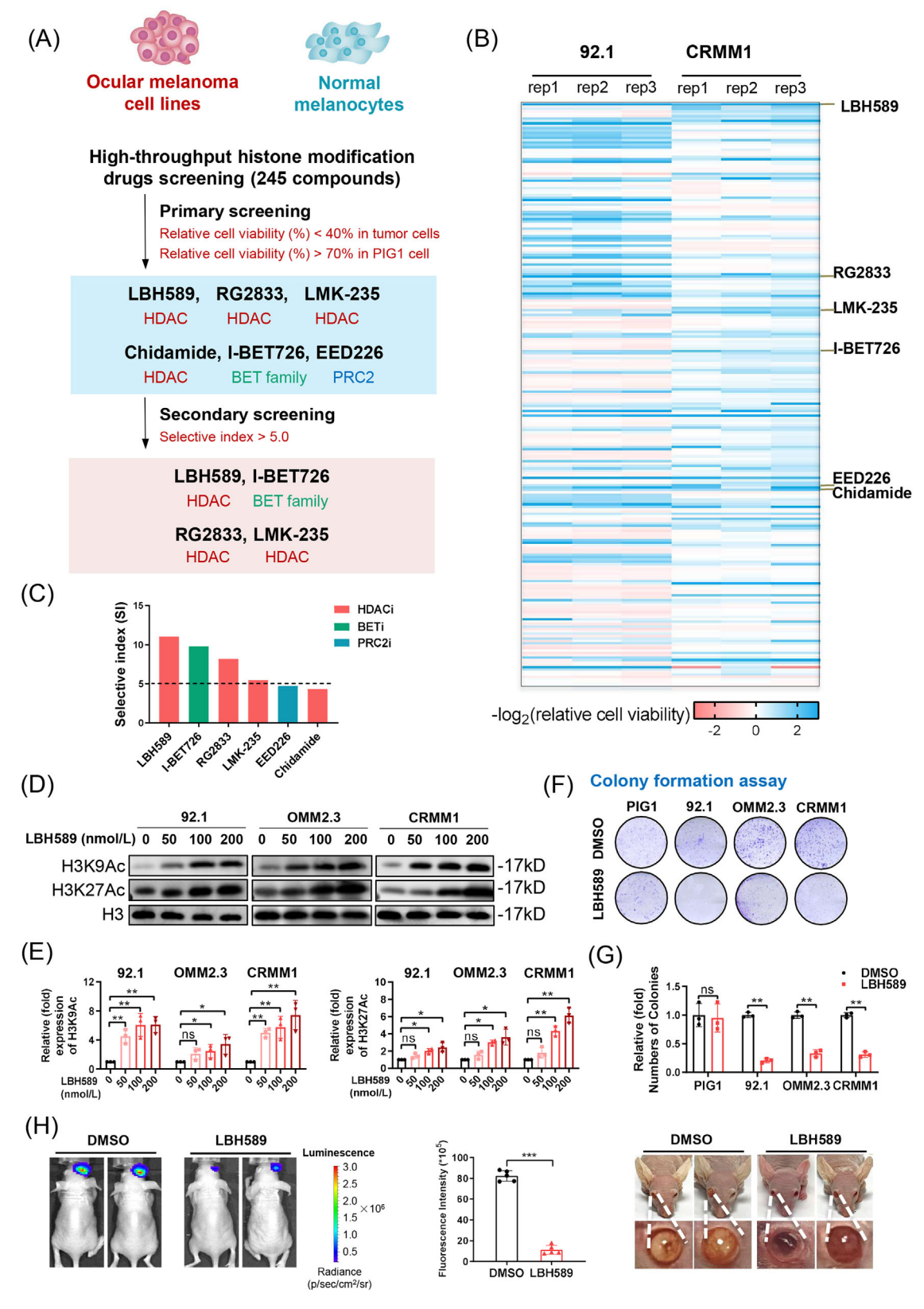


FIGURE 1 LBH589 selectively attenuates the oncogenesis of ocular melanoma. (A) Schematic diagram of high-throughput histone modification drug screening procedures. Selective index = IC_{50} (average in tumor cells) / IC_{50} (normal melanocytes). (B) Heatmap of histone modification drug screening results in ocular melanoma cell lines (92.1 and CRMM1) upon treatment with DMSO or inhibitors (100 nmol/L) for 24 h. Data represent three biological replicates. (C) Selective indices of the six histone modification inhibitor candidates (LBH589, I-BET726, RG2833, LMK-235, EED226, and Chidamide) for ocular melanoma cells. Each of these six inhibitors exhibited an inhibitory rate

selectively inhibits malignant behavior in ocular melanoma both in vitro and in vitro.

3.2 | HDAC activated m⁶A modification via induction of METTL14 expression

To explore the downstream targets of LBH589, we performed a high-throughput transcriptome analysis after treating 92.1 cells with LBH589 (Figure 2A, deposited in the GEO database, GSE214457). RNA-seq data showed a dramatic transcriptional change, with 2,841 upregulated and 2,086 downregulated genes. Notably, these downregulated genes were mainly enriched in cell cycle, cell division, and DNA replication processes, which supports the LBH589-induced inhibitory phenotype observed in ocular melanoma (Figure 2B, Supplementary Figure S3). Surprisingly, we observed that most upregulated genes (1,776/2,841,62.5%) presented with differential m⁶A methylation levels (meRIP-seq and miCLIP-seq data, GSE137675) (Figure 2C), indicating that HDAC inhibition potentially regulates global m⁶A methylation patterns. We then measured global m⁶A methylation levels using a dot blot assay. We observed a decreased m⁶A methylation level in melanoma cells than in normal melanocytes (Figure 2D), which is consistent with other m⁶A findings in melanomas [14, 21, 23]. More importantly, we found that global m⁶A methylation increased following treatment with LBH589 in ocular melanoma cells (Figure 2E) than in cutaneous melanoma cells (Supplementary Figure S4). These findings indicate that HDAC inhibition restores m⁶A methylation levels in ocular melanomas.

We then explored the molecular mechanism underlying the LBH589-induced activation of m⁶A methylation. We listed the RNA-seq data of m⁶A-related modifying enzymes, including writer proteins (*METTL3*, *METTL14*, and *WTAP*), eraser proteins (*ALKBH5* and *FTO*), and reader proteins (*YTHDF1-3*) (Figure 2F). The results indicated that *METTL14* was significantly increased in LBH589-treated melanoma cells; however, other m⁶A-related modifying enzymes remained unchanged (Figure 2G-H). Importantly, METTL14 was activated at both the mRNA (Supplementary Figure S5) and protein levels (Figure 2I). Taken together, these data indicate that HDAC inhibition induced a significant upregulation of METTL14, resulting in activation of the global m⁶A methylation level in ocular melanoma.

3.3 | METTL14 was hypo-acetylated in ocular melanoma

As METTL14 is involved in LBH589-mediated m⁶A activation, we tested the acetylation status and expression level of METTL14 in ocular melanoma. Since HDACis play an important role in the regulation of histone acetylation [32], we performed high-throughput H3K27Ac (GSE214464) and H3K9Ac (GSE162573) CUT&Tag to determine the histone acetylation pattern in ocular melanoma cells (Supplementary Figure S6A). Notably, the METTL14 promoter was hypoacetylated in ocular melanomas, as demonstrated by H3K27Ac (Figure 3A) and H3K9Ac CUT&Tag (Supplementary Figure S6B). In contrast, a significant acetylation signal was observed in the normal melanocytes (PIG1). Subsequently, a ChIP assay confirmed that ocular melanoma cells exhibited decreased H3K27Ac (Figure 3B) and H3K9Ac intensity in the METTL14 promoter (Supplementary Figure S6C) compared to that in normal pigmented cells. Most importantly, HDAC inhibition further increased H3K27Ac (Figure 3C) and H3K9Ac levels of METTL14 (Supplementary Figure S6D) in ocular melanoma cells. Taken together, these findings suggest

greater than 60% in ocular melanoma cells and less than 30% in PIG1 cells. Inhibitory rate (%) = 1 - cell viability (%). (D) Western blotting of H3K9Ac and H3K27Ac relative to histone H3 in ocular melanoma cells (92.1, OMM2.3, and CRMM1) after treatment with different concentrations of LBH589 for 24 h. Data are representative of triplicate experiments. (E) Densitometric analysis of the expression levels of H3K9Ac and H3K27Ac relative to histone H3 in ocular melanoma cells (92.1, OMM2.3, and CRMM1) upon treatment with different concentrations of LBH589. Data are presented as the mean \pm SD of triplicate experiments. Significance was determined using unpaired two-tailed Student's *t*-tests. (F-G) A Colony formation assay was performed to assess the growth of normal melanocytes (PIG1) and ocular melanoma cells (92.1, OMM2.3, and CRMM1) upon treatment with LBH589 (100 nmol/L). Representative images (F) of three experimental replicates are shown. Data (G) are presented as the mean \pm standard deviation of triplicate experiments. Significance was determined using unpaired two-tailed Student's *t*-tests. (H) Images acquired with an in vivo small-animal imaging system showing the suppression of bioluminescent signals in orthotopic xenografts derived from cells pretreated with DMSO or LBH589 (100 nmol/L, 24 h) before intraocular injection. Representative images of five biological replicates are shown. *P < 0.05, **P < 0.01, ***P < 0.001. Abbreviations: HDAC, Histone deacetylase; IC $_{50}$, half maximal inhibitory concentration; BET family, bromodomain and extra-terminal family; BETi, BET inhibitor; PRC2i, polycomb repressive complex 2 inhibitor; rep, replicate; H3, histone 3; K9: lysine 9; K27: lysine 27; Ac, acetylation; DMSO, dimethylsulfoxide; ns, no significance.

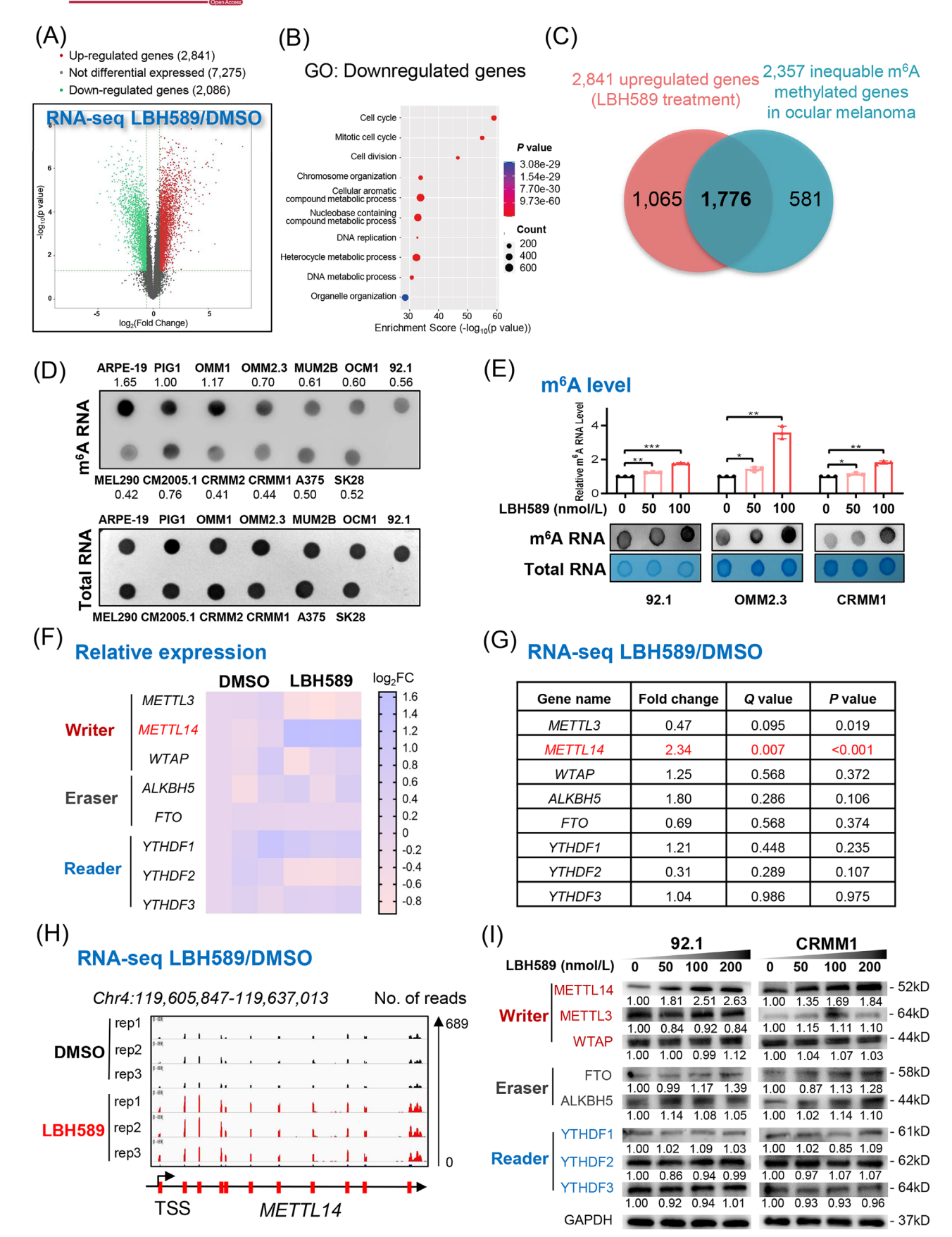


FIGURE 2 LBH589 fuels global m⁶A modification through activating METTL14. (A) Volcano plot showing 2,086 downregulated and 2,841 upregulated genes in LBH589-treated ocular melanoma cells (92.1) (\log_2 Fold Change|>1, P<0.05) compared to the control group.

that *METTL14* is hypoacetylated in ocular melanomas, which could be rescued by HDAC inhibition.

3.4 | METTL14 was downregulated and served as a tumor suppressor in ocular melanoma

We then tested the expression level of METTL14 in a patient cohort using our tissue chip [14], containing 56 ocular melanoma samples and 27 healthy human melanocytic nevi samples. Ocular melanoma exhibited downregulated METTL14 expression compared to normal nevus (Figure 3D). Data from single-cell sequencing of uveal melanoma (GSE139829, analyzed using the CancerSEA platform [33, 34]), revealed that METTL14 expression was negatively correlated with multiple oncogenic pathways, including invasion (R = -0.41, P < 0.001), metastasis (R = -0.41) 0.39, P < 0.001), epithelial-mesenchymal transition (EMT) (R = -0.27, P < 0.001), inflammation (R = -0.25, P <0.001), proliferation (R = -0.20, P < 0.001), and cell cycle (R = -0.10, P < 0.001) (Figure 3E, Supplementary Figure S7). Most importantly, elevated METTL14 expression was associated with a decreased recurrence rate in our cohort (log-rank P = 0.011) (Figure 3F). In addition, METTL14 expression was decreased in ocular melanoma cell lines, both in the RNA (Supplementary Figure S8A-B) and protein levels (Supplementary Figure S8C). Taken together, these data indicate that METTL14 serves as an important tumor suppressor in ocular melanoma.

To elucidate the role of METTL14 in the tumorigenesis of ocular melanoma, we overexpressed *METTL14* in ocular melanoma cell lines. We constructed a plasmid containing full-length *METTL14* and packaged it into a lentivirus for transfection. RNA (Supplementary Figure S9A) and protein levels of METTL14 (Supplementary

Figure S9B) were significantly upregulated in *METTL14*-overexpressing ocular melanoma cells. Following overexpression of *METTL14*, we observed a significant reduction in colony formation (Supplementary Figure S9C) and migration (Supplementary Figure S9D). We also silenced *METTL14* in ocular melanoma cells by transfecting them with two shRNAs. The two shRNAs exhibited sufficient knockdown efficacy in all ocular melanoma cell lines (Supplementary Figure S10A-B). A significant increase in colony formation (Supplementary Figure S10C) and migration ability (Supplementary Figure S10D) were observed in *METTL14*-knockdown ocular melanoma cells. Taken together, these findings suggest that METTL14 is significantly downregulated and functions as a tumor suppressor in ocular melanoma.

3.5 | HDACis suppressed ocular melanoma via activation of METTL14

To explore the role of METTL14 in LBH589-mediated tumor inhibition, we silenced METTL14 and then treated ocular melanoma cells with LBH589. We observed that LBH589-induced METTL14 activation was compromised after silencing METTL14, both in terms of RNA and protein expression levels (Figure 3G-H). After METTL14 knockdown, the extent of LBH589-mediated tumor inhibition was partially compromised, including colony formation (Figure 3I, Supplementary Figure S11A) and migration (Figure 3J, Supplementary Figure S11B). More importantly, targeted silencing of METTL14 also partially restored malignant growth in LBH589treated orthotopic xenografts (Figure 3K, Supplementary Figure S11C). Taken together, these findings indicate that METTL14-silenced cells are more resistant to HDAC inhibition.

(B) GO analysis showing the functions of the downregulated genes in ocular melanoma cells (92.1). Three biological replicates were analyzed. (C) Venn diagram showing the overlap between 2,841 genes upregulated after LBH589 treatment and 2,357 inequable m⁶A methylated genes in ocular melanoma (92.1). (D) m6A dot blot of global m6A levels in normal control cells (ARPE-19 and PIG1), ocular melanoma cells (OMM1, OMM2.3, MUM2B, OCM1, 92.1, MEL290, CM2005.1, CRMM2, and CRMM1), and cutaneous melanoma cells (A375 and SK28). (E) m⁶A dot blot of m⁶A levels in ocular melanoma cells (92.1, OMM2.3, and CRMM1) after treatment with different concentrations of LBH589 for 24 h. The images are representative of experimental triplicates. Data are presented as the mean \pm standard deviation of triplicate experiments. Significance was determined using unpaired two-tailed Student's t-tests. (F) Heatmap of the relative expression levels of m⁶A-related genes in DMSO- and LBH589-treated groups. (G) RNA-seq results showing the fold change in expression levels of m⁶A-related genes in ocular melanoma cells (92.1) after LBH589 treatment. (H) IGV tracks for METTL14 from RNA-seq data in DMSO- and LBH589-treated ocular melanoma cells (92.1). Three biological replicates were analyzed. (I)Western blotting of m⁶A-related proteins relative to GAPDH in ocular melanoma cells (92.1 and CRMM1) upon treatment with LBH589 at different concentrations. *P < 0.05, **P < 0.01, ***P < 0.001. Abbreviations: RNA-seq, RNA sequencing; GO, Gene Ontology; m⁶A, N6-methyladenine; IGV, Integrative Genomics Viewer; No., number; TSS, transcriptional start site. METTL14, methyltransferase-like 14; METTL3, methyltransferase-like 3; WTAP, Wilms tumor 1-associating protein; ALKBH5, AlkB homolog 5 RNA demethylase; FTO, fat mass and obesity-associated protein; YTHDF1, YTH N6-methyladenosine RNA binding protein 1; YTHDF2, YTH N6-methyladenosine RNA binding protein 2; YTHDF3, YTH N6-methyladenosine RNA binding protein 3; GAPDH, glyceraldehyde-3-phosphate dehydrogenase; DMSO, dimethylsulfoxide; ns, no significance.

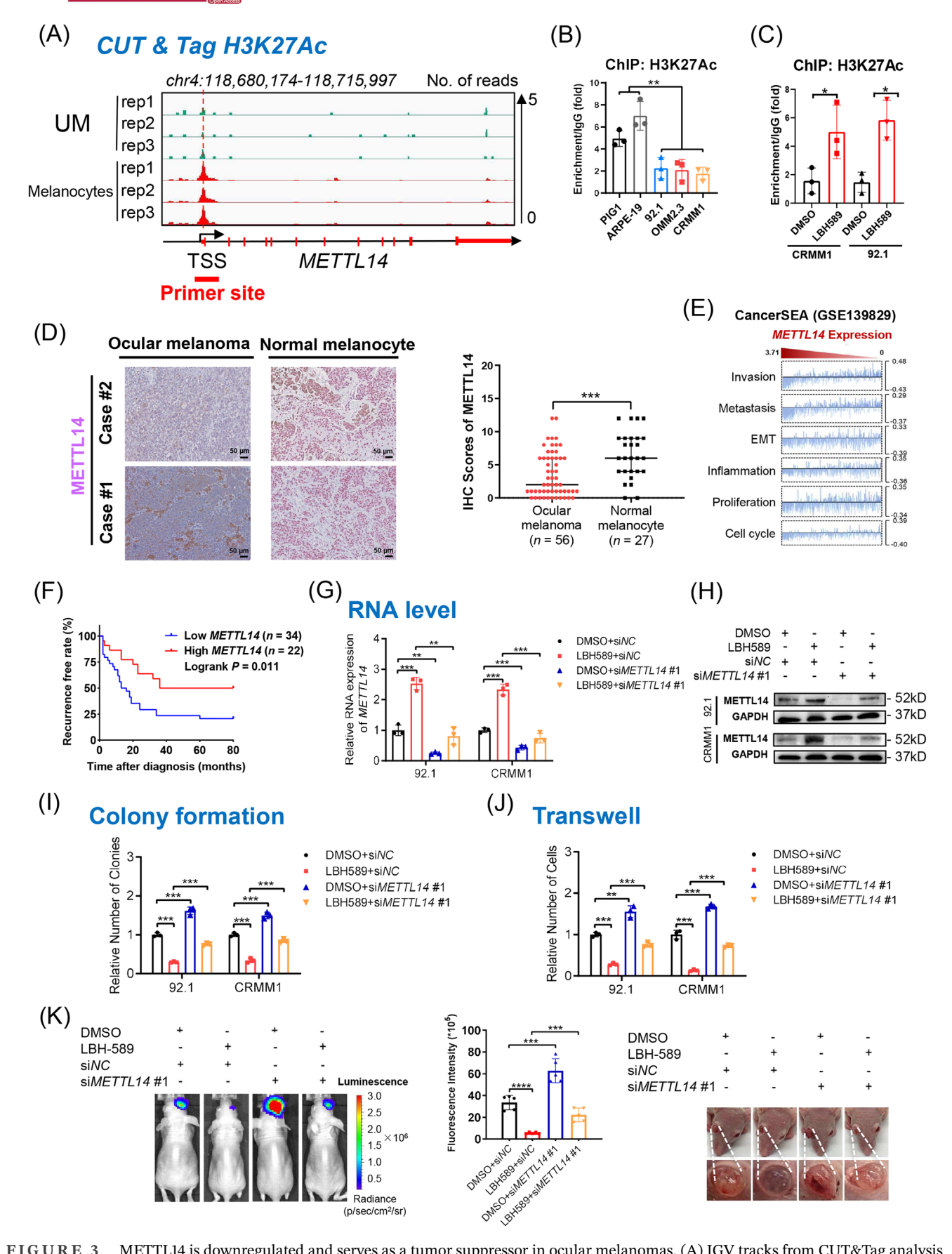


FIGURE 3 METTL14 is downregulated and serves as a tumor suppressor in ocular melanomas. (A) IGV tracks from CUT&Tag analysis showing H3K27Ac enrichment at the promoter region of *METTL14* in ocular melanoma cells and normal melanocytes. Three biological

3.6 | FAT4 is the downstream target of METTL14

We then explored the mechanism underlying the tumorsuppressive role of METTL14 in ocular melanomas. Using multi-omic analysis (Figure 4A), we identified three genes (CRYBG3, FAT4, SEMA3D) that met the following criteria: upregulated after METTL14 overexpression (blue circle, GSE215095) and LBH589 treatment (brown circle, GSE214457), positively correlated with METTL14 in TCGA cohort (red circle, R > 0.3, P < 0.05), and downregulated in tumors (green circle, GSE176345) with hypo-m⁶A modification levels (yellow circle, GSE137675). Notably, among these three genes, only FAT4 exhibited a prognostic value (Figure 4B, Supplementary Figure S12) and parallel expression with METTL14 in the TCGA cohort (R = 0.471, P < 0.001, Figure 4C). Notably, FAT4 expression was significantly increased after METTL14 overexpression (Figure 4D) and LBH589 treatment (Figure 4E), as demonstrated by the RNA-seq chromatogram. More importantly, we found that FAT4 expression was induced by LBH589 treatment and associated with METTL14 expression, both at the RNA and protein levels (Figure 4F-G). Taken together, these data indicated that FAT4 may participate in METTL14-mediated tumor inhibition in ocular melanoma.

3.7 | FAT4 acted as a tumor suppressor in ocular melanoma

Although FAT4 serves as a conventional tumor suppressor in many cancers [35-38], its function in ocular melanoma remains enigmatic. We tested the expression of FAT4 in ocular melanoma samples and cell lines. Similar to METTL14, FAT4 levels were significantly decreased in clinical samples of ocular melanoma (Figure 5A), which was associated with a reduced recurrence rate (Figure 5B). Importantly, FAT4 RNA and protein levels were also decreased in ocular melanoma cell lines (Figure 5C-E). To evaluate the role of FAT4 in METTL14-mediated tumor suppression, we silenced FAT4 expression in METTL14overexpressed ocular melanoma cell lines (Figure 5F). Interestingly, knockdown of FAT4 attenuated METTL14mediated tumor inhibition, including colony formation ability (Figure 5G, Supplementary Figure S13A) and metastasis capacity (Figure 5H, Supplementary Figure S13B). Similarly, in the orthotopic xenograft model, silencing

replicates were analyzed. (B) ChIP-qPCR assay of H3K27Ac status at the METTL14 TSS region in ocular melanoma cells (92.1, OMM2.3, and CRMM1) and normal control cells (PIG1 and ARPE-19) compared with IgG. Data are presented as the mean \pm SD of triplicate experiments. Significance was determined using unpaired two-tailed Student's t-tests. (C) ChIP-qPCR assay of H3K27Ac status at the METTL14 TSS region in ocular melanoma cells (92.1 and CRMM1) after LBH589 exposure compared to the DMSO-treated group. Data are presented as the mean \pm SD of triplicate experiments. Significance was determined using unpaired two-tailed Student's t-tests. (D) The IHC assay showed that METTL14 in ocular melanoma and normal melanocyte samples. Representative images were shown. IHC scores of METTL14 in ocular melanoma tissues (n = 56) and normal melanocyte tissues (n = 27) are presented as the median with interquartile range. Significance was determined using unpaired Mann-Whitney nonparametric test. (E) Correlation analysis of METTL14 expression and functional states in single-cell datasets from CancerSEA (GSE139829). Significance was determined using Pearson correlation analysis (filtered by correlation strength < -0.1, P < 0.001). (F) Kaplan-Meier analysis of the correlation between IHC scores of METTL14 and recurrence-free rate in the internal cohort (n = 56). Significance was determined by a two-sided log-rank test. (G) qPCR data showing METTL14 expression in ocular melanoma cells (92.1 and CRMM1) after DMSO or LBH589 exposure in METTL14 knockdown or control groups, respectively. Data are presented as the mean \pm SD of triplicate experiments. Significance was determined using unpaired two-tailed Student's t-tests. (H) Western blotting of METTL14 relative to GAPDH in ocular melanoma cells (92.1 and CRMM1) after DMSO or LBH589 exposure in METTL14 knockdown or control groups, respectively. The images are representative of experimental triplicates. (I) A colony formation assay was performed to assess the growth of ocular melanoma cells (92.1 and CRMM1) upon DMSO or LBH589 treatment in METTL14 knockdown or control groups, respectively. The colony formation assay data are presented as the mean \pm SD of triplicate experiments. Significance was determined using unpaired two-tailed Student's t-tests. (J) A transwell assay was performed to assess the cell migration ability of ocular melanoma cells (92.1 and CRMM1) upon DMSO or LBH589 treatment in METTL14 knockdown or control groups, respectively. Data are presented as the mean ± SD of triplicate experiments. Significance was determined using unpaired two-tailed Student's t-tests. (K) Images acquired with an in vitro small animal imaging system showing bioluminescent signals in orthotopic xenografts derived from 92.1 cells upon DMSO or LBH589 (100 nmol/L, 24 h) treatment in METTL14 knockdown or control groups, respectively. Representative images of five biological replicates are shown. Data are presented as the mean \pm SEM. The overall and eyeball appearances exhibited tumor volumes in the orthotopic xenografts. *P < 0.05, *P < 0.01, *P < 0.001. Abbreviations: UM, uveal melanoma; CUT&Tag, Cleavage Under Targets and Tagmentation; No., number; rep, replicate; METTL14, methyltransferase-like 14; IGV, Integrative Genomics Viewer; NC, normal control; H3K27Ac, acetylation of histone 3 at lysine 27; ChIP, Chromatin immunoprecipitation; qPCR, quantitative real-time polymerase chain reaction; TSS, transcriptional start site; EMT, epithelial-mesenchymal transition; SD, standard deviation; SEM, standard error of mean; DMSO, dimethylsulfoxide; IHC, immunohistochemistry; GAPDH, glyceraldehyde-3-phosphate dehydrogenase.

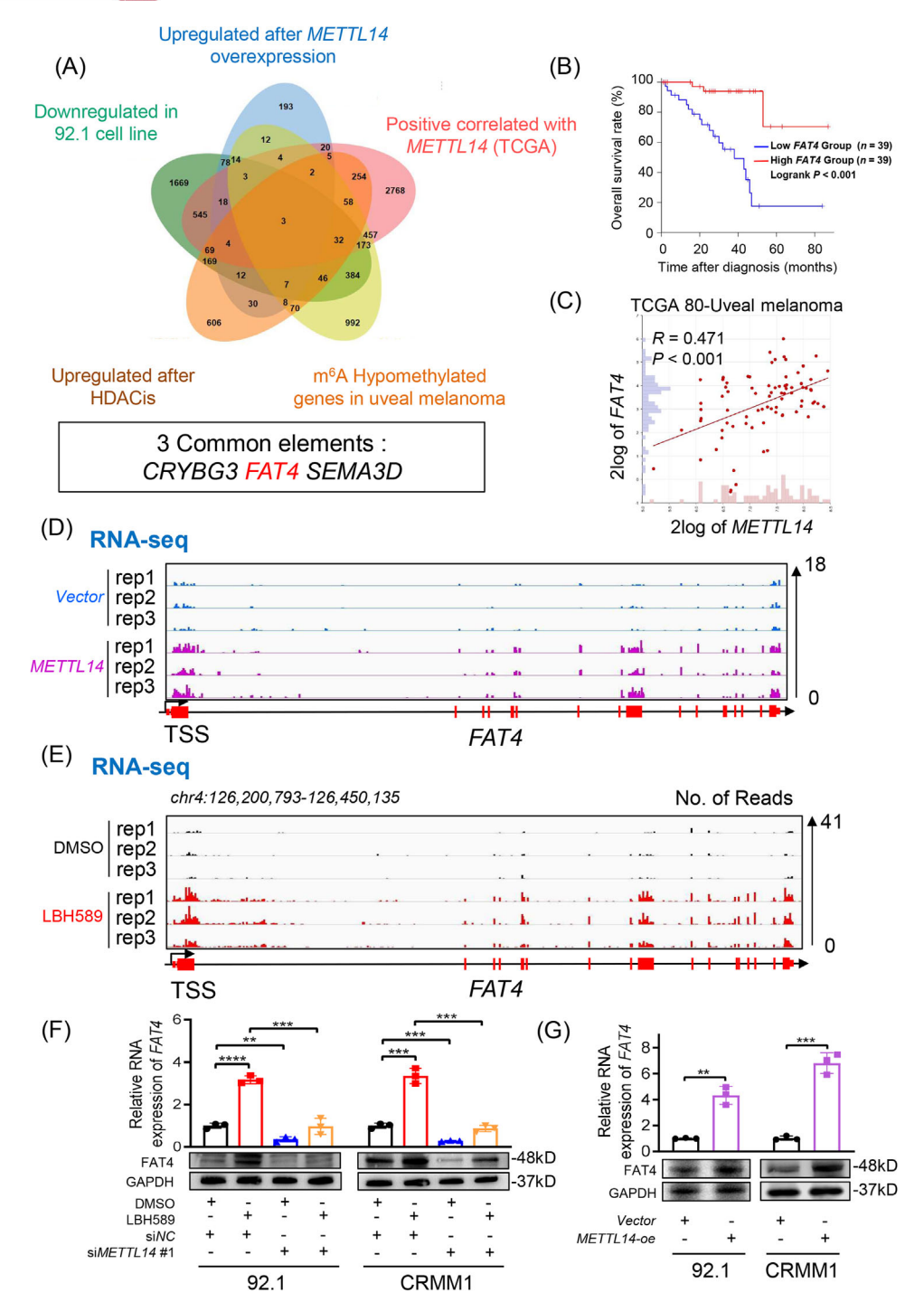


FIGURE 4 FAT4 serves as the downstream candidate of METTL14. (A) Venn diagram identifying *CRYBG3*, *FAT4*, and *SEMA3D* as downstream target candidates of METTL14. (B) Kaplan-Meier analysis showing the correlation between *METTL14* expression and overall survival in TCGA-uveal melanoma patients stratified by *METTL14* expression levels. Statistical significance was determined using a two-sided log-rank test. (C) Correlation analysis of *METTL14* and *FAT4* expression in the TCGA-uveal melanoma cohort. Significance was determined using *Pearson*'s correlation analysis (R = 0.471, P < 0.001). (D) IGV tracks for *FAT4* from RNA-seq data in the control and *METTL14*-overexpressed ocular melanoma cell lines. Biological triplicates were analyzed. (E) IGV tracks for *FAT4* from RNA-seq data in control and LBH589-treated ocular melanoma cell lines. Biological triplicates were analyzed. (F) Real-time PCR (top) data showing *FAT4* expression in ocular melanoma cells (92.1 and CRMM1) after DMSO or LBH589 treatment in *METTL14* knockdown group and control group, respectively. Data are presented as the mean ± SD of triplicate experiments. Significance was determined using unpaired two-tailed Student's *t*-tests. Western blotting (bottom) of FAT4 relative to GAPDH in ocular melanoma cells (92.1 and CRMM1) after DMSO or LBH589 treatment in *METTL14* knockdown group and control group, respectively. Representative images from three experimental replicates are shown. (G) Real-time PCR (top) data showing *FAT4* expression in control and *METTL14*-overexpressed ocular melanoma cells (92.1 and CRMM1). Western blotting (bottom) of FAT4 relative to GAPDH in control and *METTL14*-overexpressed ocular melanoma cells (92.1 and CRMM1). Data

of *FAT4* counteracted *METTL14* overexpression-induced tumor inhibition (Figure 5I, Supplementary Figure S13C). Taken together, these results indicate that FAT4 participates in the inhibitory network mediated by METTL14 in ocular melanoma.

3.8 | YTHDF1 recognition of m⁶A modification enhanced RNA stability of FAT4

Since METTL14 is responsible for "writing" m⁶A modification, we next tested whether FAT4 expression was modulated by METTL14 in an m⁶A modification-dependent manner. Congruent with the fact that METTL14 was expressed at low levels in these cells, we found that *FAT4* was hypomethylated in ocular melanoma cell lines using miCLIP-seq (Figure 6A) and meRIP-seq (Figure 6B). Moreover, using RIP, we found that *FAT4* was significantly hypo-m⁶A-methylated in ocular melanoma cells (Supplementary Figure S14A). Importantly, exogenous *METTL14* expression further increased the m⁶A methylation levels of *FAT4* (Supplementary Figure S14B). Taken together, these data indicate that METTL14 is responsible for catalyzing m⁶A methylation of *FAT4* mRNA.

As YTHDF family proteins are responsible for the recognition of m⁶A methylation, which plays an important role in determining their RNA fate [10, 39], we then explored the function of these "readers" in FAT4 regulation. Using RIP-PCR, we found that FAT4 mRNA specifically bound to YTHDF1 in both normal melanocytes and METTL14-overexpressed ocular melanoma cells, while a weak interaction signal was observed between other reader proteins (YTHDF2 and 3) and FAT4 mRNA (Figure 6C). Consequently, silencing YTHDF1 significantly inhibited FAT4 expression, whereas FAT4 expression remained unchanged in YTHDF2/3-silenced cells (Figure 6D). Interestingly, exogenous expression of METTL14 increased the stability of FAT4 mRNA, which was associated with elevated expression of FAT4 in METTL14-overexpressed cells (Figure 6E, purple). Moreover, silencing of YTHDF1 significantly impaired FAT4 RNA stability (Figure 6E, brown) and abrogated METTL14-mediated function (Figure 6E, green). Interestingly, a significant positive correlation was observed between FAT4 and YTHDF1 (R = 0.359, P <

0.001) (Figure 6F). These findings indicated that YTHDF1 promotes FAT4 expression, which depends on METTL14-mediated m⁶A modification (Figure 6G).

4 | DISCUSSION

HDACis are the first epigenetic drugs used in cancer treatment, making them the largest group of United States Food and Drug Administration-approved epidrugs [40, 41]. Although HDACis exhibit anti-cancer activity in both in vitro and in vitro models of ocular melanoma, the underlying mechanism remains to be fully elucidated. For example, HDACis significantly inhibited the proliferation and metastasis and promoted apoptosis of ocular melanoma cells [42]. Moreover, HDAC inhibition increased human leukocyte antigen class I expression in uveal melanoma, demonstrating that HDACis potentially influenced the outcome of immunotherapy [43]. Furthermore, HDACis selectively inhibited the Wnt/ β -catenin pathway and downregulated the percentage of aldehyde dehydrogenase activity-positive cells, leading to a decrease in cancer stemness [30]. In this study, we revealed that METTL14 was a downstream factor involved in the anticancer efficacy exhibited by LBH589 in ocular melanoma, which indicated that m⁶A is dynamically regulated by histone acetylation.

m⁶A methylation is the most prevalent mRNA modification that occurs in almost every category of eukaryotes. Aberrant m⁶A modifications were frequently identified in many cancers, including melanoma [14], cervical cancer [44], lung cancer [45], and colon cancer [46]. Notably, several studies showed that m⁶A hypomethylation supported melanoma tumorigenesis and progression, particularly in metabolic reprogramming and resistance towards anti-PD-1 blockade [20–23].

In this study, we identified that *METTL14* was silenced by hypo-histone-acetylation in ocular melanoma. Notably, after silencing *METTL14*, the extent of HDACi-mediated tumor inhibition was partially compromised, both in vitro and in vitro. We found that *METTL14*-silenced cells were more resistant to HDAC inhibition compared to control cells. This finding agreed with the tumor-suppressor function of METTL14 and previously reported single-cell analysis data [34, 47-49]. Also, this indicated that LBH589

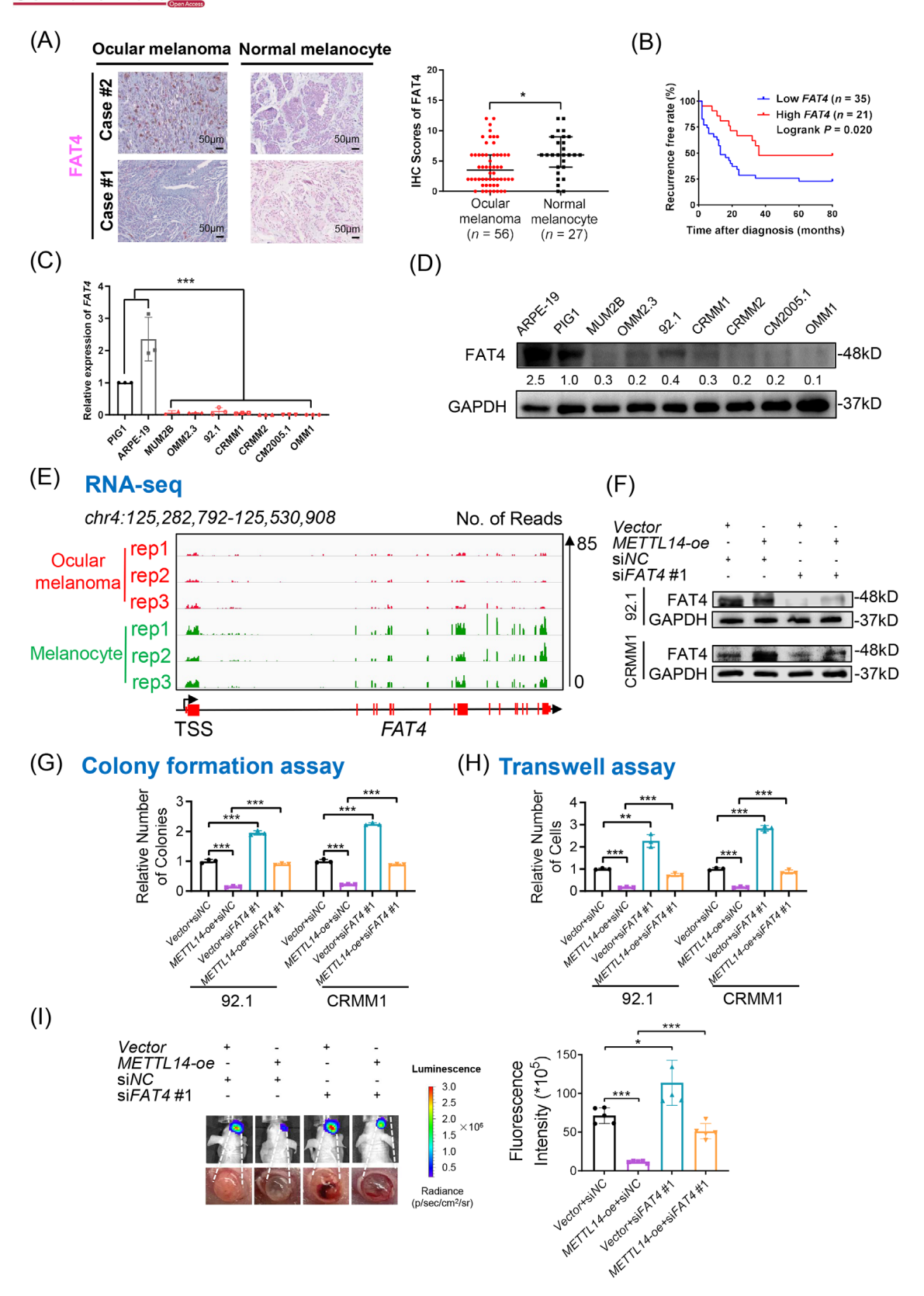


FIGURE 5 FAT4 acts as a tumor suppressor. (A) The IHC assay showed that FAT4 in ocular melanoma and normal melanocyte samples. Representative images were shown. IHC scores of FAT4 in ocular melanoma tissues (n = 56) and normal melanocyte tissues (n = 27) are presented as the median with interquartile range. Significance was determined using unpaired Mann-Whitney nonparametric test. (B) Kaplan–Meier analysis of the correlation between IHC scores of FAT4 and recurrence-free rate in the internal cohort (n = 56). Significance was determined by a two-sided log-rank test. (C) Real-time PCR data showing the expression levels of *FAT4* in ocular melanoma cell lines and

exerted its anticancer effect not only in an m⁶A-dependent manner but also possibly by other downstream effectors.

In this study, we also found that the m⁶A methylation level was decreased in cutaneous melanoma cells (A375 and SK28), but it was not increased following treatment with LBH589. We speculated that m⁶A methylation was not the downstream targets of HDACis in cutaneous melanoma. Previous studies revealed that HDACis suppressed proliferation, apoptosis, and migration of cutaneous melanoma cells [50-52], suggesting that HDACis prevented cutaneous melanoma progression independent of m⁶A methylation. For example, HDACis disrupted HDAC6-protein phosphatase 1 (PP1) complex to release the active PP1 that dephosphorylated protein kinase B and blocked its carcinogenic signaling in cutaneous melanoma [53]. The HDACi ITF2357 targeted b-raf protooncogene (BRAF) in melanoma cells, induced a switch from autophagy to classic apoptosis, and reduced the viability of BRAF-mutated melanoma cells [54]. The YTHDF family, m⁶A reader proteins, recognize and bind to m⁶Amodified genes to regulate their expression through modulating mRNA structure, mRNA splicing, mRNA stability, mRNA export and translation efficiency [12, 55]. It was known that YTHDF1 could improve translation by interacting with ribosomes and translation-initiating factors [56]. In our study, the results demonstrated that YTHDF1 recognized the m⁶A modification of FAT4 mRNA and enhanced FAT4 mRNA stability, thus enhancing FAT4 expression. Notably, YTHDF1 may enhance expression of target molecules through the promotion of the translation capacity, which awaits further explorations.

FAT4 belongs to the FAT protein family, which was first identified as a tumor suppressor in mammals. FAT4 exerted onco-suppressive roles in multiple malignant tumors, including colorectal cancer [57], gastric cancer

[58] and esophageal squamous cell carcinoma [59] and prevented various oncogenic events, involving EMT and stemness promotion [54, 59]. For example, FAT4 mediated the activity of phosphoinositide-3 kinase (PI3K) to stimulate autophagy, suppressed EMT and inhibited tumor progression in colorectal cancer [57]. FAT4 activation triggered Hippo signaling and constrained yesassociated protein nuclear translocation to arrest cell cycle, suppressed cell proliferation, prevented stemness and promoted senescence in lung cancer [54]. In this study, we revealed that the METTL14/FAT4 signaling cascade was important for tumor suppression in ocular melanoma. Generally, HDACis partially restored the histone acetylation level of METTL14 and thereby induced FAT4-mediated tumor-suppressive signaling pathways in ocular melanoma (Figure 7). Therefore, a "targeted m⁶A reprogramming strategy" provided an avenue to explore epigenome dynamics during tumorigenesis.

The limitations of this study were as follows. Firstly, in our study, the HDACi/METTL14/FAT4 signaling cascade was established based on immortal cell lines, which awaits further validation by using primary ocular melanoma cells. Secondly, the intraocular xenograft model was constructed using ocular melanoma cell lines, which may be different from clinical patient samples. Thirdly, some data were validated using clinical samples, but the cohort size was small, and there was no match between the tumor group and the normal control group. Lastly, this study found that HDACi up-regulated the m⁶A modification level of FAT4 by activating METTL14, promoted the expression of FAT4 and inhibited the growth of ocular melanoma, but other possible downstream effector molecules of HDACi were not explored. The above problems can be further explored and solved in the follow-up study.

retinal pigment epithelial cells, relative to normal melanocytes. Data are presented as the mean \pm SD of triplicate experiments. Significance was determined using unpaired two-tailed Student's t-tests. (D) Western blotting of FAT4 relative to GAPDH in ocular melanoma cells, retinal pigment epithelial cells, and normal melanocytes. The images are representative of experimental triplicates. (E) Integrative Genomics Viewer tracks showing the expression levels of FAT4 from RNA-seq data in ocular melanoma cells and normal melanocytes. The biological triplicates were analyzed. (F) Western blotting of FAT4 relative to GAPDH in control or METTL14-overexpressed ocular melanoma cells (92.1 and CRMM1) upon FAT4 knockdown or not. The images are representative of experimental triplicates. (G) A colony formation assay was performed to assess the growth of control or METTL14-overexpressed ocular melanoma cells (92.1 and CRMM1) upon FAT4 knockdown. Data are presented as the mean ± SD of triplicate experiments. Significance was determined using unpaired two-tailed Student's t-tests. (H) A transwell assay was performed to assess the cell migration ability of control or METTL14-overexpressed ocular melanoma cells (92.1 and CRMM1) upon FAT4 knockdown. Data are presented as the mean \pm SD of triplicate experiments. Significance was determined using unpaired two-tailed Student's t-tests. (I) Representative images from five biological replicates showing the bioluminescent signals (top) and eyeball appearances (bottom) of orthotopic xenografts derived from control or METTL14-overexpressed ocular melanoma cells (92.1 and CRMM1) upon FAT4 knockdown. Data are presented as the mean \pm SEM. *P < 0.05, **P < 0.01, ***P < 0.001. Abbreviations: FAT4, FAT Tumor Suppressor Homolog 4; IHC, immunohistochemistry; GAPDH, glyceraldehyde-3-phosphate dehydrogenase; SD, standard deviation; RNA-seq, RNA sequencing; rep, replicate; TSS, transcriptional start site; No., number; METTL14, methyltransferase-like 14; NC, normal control; oe, overexpression; SEM, standard error of mean.

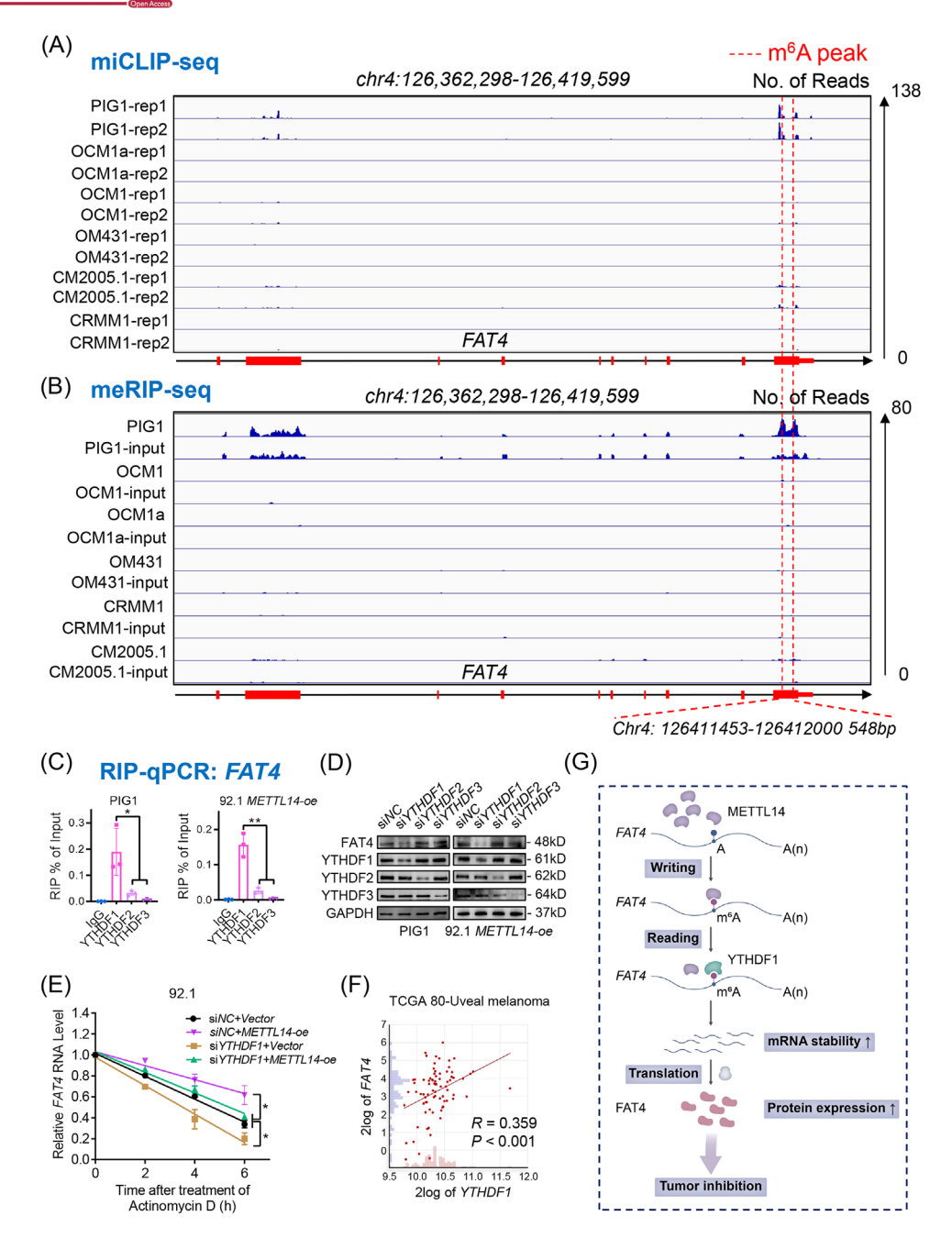


FIGURE 6 The YTHDF1 recognition of FAT4 m⁶A modification enhances RNA stability. (A-B) Integrative Genomics Viewer tracks showing m⁶A status at FAT4 from miCLIP-seq (A) and meRIP-seq (B) data in ocular melanoma cells and normal melanocytes. (C) RIP-qPCR assay of YTHDF1, YTHDF2, and YTHDF3 status in the transcripts of METTL14 in ocular melanoma cells (92.1) and normal melanocytes (PIG1). Data are presented as the mean \pm SD of triplicate experiments, (D) Western blotting of FAT4, YTHDF1, YTHDF2, and YTHDF3 relative to GAPDH in control or YTHDF1/2/3 knockdown ocular melanoma cells (92.1) and normal melanocytes (PIG1). (E) Lifetime FAT4 mRNA levels in control or METTL14-overexpressed ocular melanoma cells upon YTHDF1 silencing. (F) Correlation analysis of FAT4 expression and YTHDF1 expression in TCGA-uveal melanoma cohort. Statistical significance was determined using Pearson's correlation analysis (R = 0.359, P < 0.01). (G) Schematic diagram of the regulatory mechanism by which METTL14 functions as a tumor suppressor in ocular melanoma. METTL14 deposits m⁶A modifications in FAT4 transcripts YTHDF1 recognizes m⁶A modification sites in FAT4 mRNA and enhances its stability, which facilitates the expression of FAT4 protein. *P < 0.05, **P < 0.01. Abbreviations: FAT4, FAT Tumor Suppressor Homolog 4; rep, replicate; m⁶A, N6-methyladenine; meRIP-seq, methylated RNA immunoprecipitation sequencing; miCLIP-seq, m⁶A individual-nucleotide-resolution cross-linking and immunoprecipitation; No. number; RIP, RNA-binding protein immunoprecipitation; qPCR, quantitative real-time polymerase chain reaction; YTHDF1, YTH N6-methyladenosine RNA binding protein 1; YTHDF2, YTH N6-methyladenosine RNA binding protein 2; YTHDF3, YTH N6-methyladenosine RNA binding protein 3; METTL14, methyltransferase-like 14; NC, normal control; oe, overexpression; SD, standard deviation; GAPDH, glyceraldehyde-3-phosphate dehydrogenase; TCGA, The Cancer Genome Atlas.

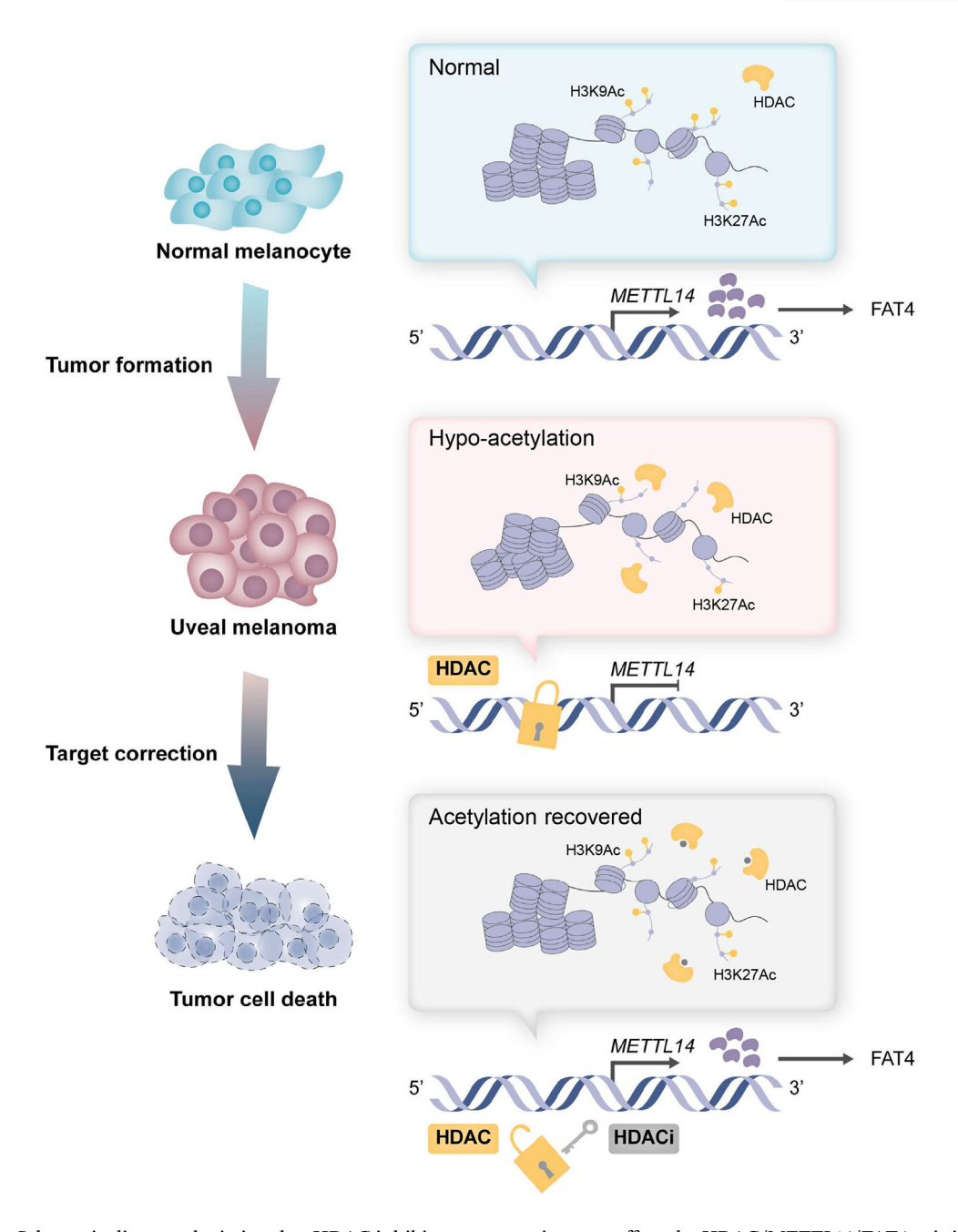


FIGURE 7 Schematic diagram depicting that HDAC inhibitors exert anti-cancer effects by HDAC/METTL14/FAT4 axis in ocular melanoma. In normal melanocytes, histone acetylation (H3K9Ac and H3K27Ac) at the transcription start site maintains the transcription of *METTL14*. Aberrant hypoacetylation "locks" the expression of *METTL14*, which contributes to the tumorigenesis of uveal melanoma. Target correction by the pan-HDAC inhibitor, LBH589, which acts as an "unlocking key" to restore the acetylation levels of histone H3 at the transcription start site of *METTL14*, exerts a potent anti-tumor effect. Abbreviations: H3, histone 3; H3K9Ac, acetylation of histone 3 at lysine 9; H3K27Ac, acetylation of histone 3 at lysine 27; HDAC, histone deacetylase; HDACi, histone deacetylase inhibitor; METTL14, methyltransferase-like 14; FAT4, FAT Tumor Suppressor Homolog 4.

5 | CONCLUSIONS

Taken together, our study revealed that histone acetylation was an important regulator of the m⁶A methylation landscape in ocular melanoma. LBH589 inhibited HDACs and activated histone acetylation of *METTL14*, which subsequently mediated m⁶A modification in tumorigenesis. In

addition, METTL14 served as a tumor suppressor by promoting the expression of FAT4, a tumor suppressor, in an $\rm m^6A\text{-}YTHDF1\text{-}dependent}$ manner. These results revealed the mechanism by which the HDACi LBH589 inhibited cancer progression via reprogramming $\rm m^6A$ methylation, unveiling a novel histone-RNA crosstalk epigenetic mechanism in the oncogenesis of ocular melanoma.



DECLARATIONS

AUTHOR CONTRIBUTIONS

XQF, RBJ and PWC designed the research, supervised the experiments, and approved the manuscript. AZ performed the experiments with assistance from XG and SYW; AZ, TXG and SFG performed the bioinformatics analyses and contributed to the experimental candidate selection; AZ, PWC and TXG analyzed the data and drafted the manuscript. All the authors read and approved this manuscript.

ACKNOWLEDGMENTS

We thank all the uveal melanoma and conjunctival melanoma patients enrolled in our study and wish them good health. This work was supported by the National Natural Science Foundation of China (82103240), the Science and Technology Commission of Shanghai (20DZ2270800, 23ZR1438400, 23ZR1480100 and 23YF1422400), Shanghai Key Clinical Specialty, Shanghai Eye Disease Research Center (2022ZZ01003), Cross-disciplinary Research Fund of Shanghai Ninth People's Hospital, Shanghai Jiao Tong University (JYJC202210 and YG2023QNB15), and Innovative Research Team of High-level Local Universities in Shanghai (SHSMU-ZDCX20210900, SHSMU-ZDCX20210902).

CONFLICT OF INTEREST STATEMENT

No potential conflicts of interest were reported by the authors.

ETHICS APPROVAL AND CONSENT TO PARTICIPATE

This research was performed in accordance with the World Medical Association Declaration of Helsinki. The use of tissue specimens was approved by the Ethics Committee of Shanghai Ninth People's Hospital affiliated to Shanghai Jiao Tong University School of Medicine (SH9H-2019-T185-2). The animal experiments were approved by the Experimental Animal Ethics Committee of Shanghai Ninth People's Hospital affiliated to Shanghai Jiao Tong University School of Medicine (SH9H-2021-A058-SB). The written permission was obtained from all patients.

CONSENT FOR PUBLICATION

Not applicable.

DATA AVAILABILITY STATEMENT

The raw sequence data reported in this paper, CUT&Tag of H3K9Ac and H3K27Ac data, have been deposited in the Gene Expression Omnibus database under accession number GSE176345, GSE214457, GSE137675, GSE215095, GSE214464, and GSE162573.

ORCID

Ai Zhuang https://orcid.org/0000-0002-7101-371X

Peiwei Chai https://orcid.org/0000-0002-9135-0940

Renbing Jia https://orcid.org/0000-0001-6642-7451

Xiangun Fan https://orcid.org/0000-0002-9394-3969

REFERENCES

- Shvedunova M, Akhtar A. Modulation of cellular processes by histone and non-histone protein acetylation. Nat Rev Mol Cell Biol. 2022;23(5):329–49.
- 2. Zhao S, Allis CD, Wang GG. The language of chromatin modification in human cancers. Nat Rev Cancer. 2021;21(7):413–30.
- 3. Liu X, Wang Y, Lu H, Li J, Yan X, Xiao M, et al. Genomewide analysis identifies NR4A1 as a key mediator of T cell dysfunction. Nature. 2019;567(7749):525–9.
- Zeleke TZ, Pan Q, Chiuzan C, Onishi M, Li Y, Tan H, et al. Network-based assessment of HDAC6 activity predicts preclinical and clinical responses to the HDAC6 inhibitor ricolinostat in breast cancer. Nat Cancer. 2023;4(2):257–75.
- 5. Hellmann MD, Jänne PA, Opyrchal M, Hafez N, Raez LE, Gabrilovich DI, et al. Entinostat plus Pembrolizumab in Patients with Metastatic NSCLC Previously Treated with Anti-PD-(L)1 Therapy. Clin Cancer Res. 2021;27(4):1019–28.
- Ny L, Jespersen H, Karlsson J, Alsén S, Filges S, All-Eriksson C, et al. The PEMDAC phase 2 study of pembrolizumab and entinostat in patients with metastatic uveal melanoma. Nat Commun. 2021;12(1):5155.
- Faião-Flores F, Emmons MF, Durante MA, Kinose F, Saha B, Fang B, et al. HDAC Inhibition Enhances the In Vivo Efficacy of MEK Inhibitor Therapy in Uveal Melanoma. Clin Cancer Res. 2019;25(18):5686–701.
- Zhao BS, Roundtree IA, He C. Post-transcriptional gene regulation by mRNA modifications. Nat Rev Mol Cell Biol. 2017;18(1):31–42.
- Dong S, Wu Y, Liu Y, Weng H, Huang H. N(6) -methyladenosine Steers RNA Metabolism and Regulation in Cancer. Cancer Commun (Lond). 2021;41(7):538–59.
- Zaccara S, Ries RJ, Jaffrey SR. Reading, writing and erasing mRNA methylation. Nat Rev Mol Cell Biol. 2019;20(10):608–24.
- 11. He PC, He C. m(6) A RNA methylation: from mechanisms to therapeutic potential. Embo j. 2021;40(3):e105977.
- 12. Jiang X, Liu B, Nie Z, Duan L, Xiong Q, Jin Z, et al. The role of m6A modification in the biological functions and diseases. Signal Transduct Target Ther. 2021;6(1):74.
- Han D, Liu J, Chen C, Dong L, Liu Y, Chang R, et al. Antitumour immunity controlled through mRNA m(6)A methylation and YTHDF1 in dendritic cells. Nature. 2019;566(7743):270– 4.
- Jia R, Chai P, Wang S, Sun B, Xu Y, Yang Y, et al. m(6)A modification suppresses ocular melanoma through modulating HINT2 mRNA translation. Mol Cancer. 2019;18(1):161.
- Jager MJ, Shields CL, Cebulla CM, Abdel-Rahman MH, Grossniklaus HE, Stern MH, et al. Uveal melanoma. Nat Rev Dis Primers. 2020;6(1):24.
- 16. Brouwer NJ, Verdijk RM, Heegaard S, Marinkovic M, Esmaeli B, Jager MJ. Conjunctival melanoma: New insights in tumour genetics and immunology, leading to new therapeutic options. Prog Retin Eye Res. 2022;86:100971.

- 17. Chai P, Jia R, Li Y, Zhou C, Gu X, Yang L, et al. Regulation of epigenetic homeostasis in uveal melanoma and retinoblastoma. Prog Retin Eye Res. 2022;89:101030.
- Landreville S, Agapova OA, Matatall KA, Kneass ZT, Onken MD, Lee RS, et al. Histone deacetylase inhibitors induce growth arrest and differentiation in uveal melanoma. Clin Cancer Res. 2012;18(2):408–16.
- Cunneen TS, Conway RM, Madigan MC. In vitro effects of histone deacetylase inhibitors and mitomycin C on tenon capsule fibroblasts and conjunctival melanoma cells. Arch Ophthalmol. 2009;127(4):414–20.
- 20. Liu Y, Liang G, Xu H, Dong W, Dong Z, Qiu Z, et al. Tumors exploit FTO-mediated regulation of glycolytic metabolism to evade immune surveillance. Cell Metab. 2021;33(6):1221–33.e11.
- 21. Yang S, Wei J, Cui YH, Park G, Shah P, Deng Y, et al. m(6)A mRNA demethylase FTO regulates melanoma tumorigenicity and response to anti-PD-1 blockade. Nat Commun. 2019;10(1):2782.
- 22. Wang L, Hui H, Agrawal K, Kang Y, Li N, Tang R, et al. m(6) A RNA methyltransferases METTL3/14 regulate immune responses to anti-PD-1 therapy. Embo j. 2020;39(20):e104514.
- Li N, Kang Y, Wang L, Huff S, Tang R, Hui H, et al. ALKBH5 regulates anti-PD-1 therapy response by modulating lactate and suppressive immune cell accumulation in tumor microenvironment. Proc Natl Acad Sci U S A. 2020;117(33):20159–70.
- 24. Qi Y, Yao R, Zhang W, Cui Q. KAT1 triggers YTHDF2-mediated ITGB1 mRNA instability to alleviate the progression of diabetic retinopathy. Pharmacol Res. 2021;170:105713.
- 25. Gu X, Hua Y, Yu J, Yang L, Ge S, Jia R, et al. Epigenetic drug library screening reveals targeting DOT1L abrogates NAD(+) synthesis by reprogramming H3K79 methylation in uveal melanoma. J Pharm Anal. 2023;13(1):24–38.
- 26. Lyu J, Yang EJ, Zhang B, Wu C, Pardeshi L, Shi C, et al. Synthetic lethality of RB1 and aurora A is driven by stathmin-mediated disruption of microtubule dynamics. Nat Commun. 2020;11(1):5105.
- Kaya-Okur HS, Wu SJ, Codomo CA, Pledger ES, Bryson TD, Henikoff JG, et al. CUT&Tag for efficient epigenomic profiling of small samples and single cells. Nat Commun. 2019;10(1):1930.
- Zhou C, Wen X, Ding Y, Ding J, Jin M, Liu Z, et al. Eye-preserving therapies for advanced retinoblastoma: a multicenter cohort of 1678 patients in China. Ophthalmology. 2022;129(2):209–19.
- 29. Xu Y, He X, Wang S, Sun B, Jia R, Chai P, et al. The m(6)A reading protein YTHDF3 potentiates tumorigenicity of cancer stem-like cells in ocular melanoma through facilitating CTNNB1 translation. Oncogene. 2022;41(9):1281–97.
- Wang Y, Liu M, Jin Y, Jiang S, Pan J. In vitro and in vivo anti-uveal melanoma activity of JSL-1, a novel HDAC inhibitor. Cancer Lett. 2017;400:47–60.
- 31. Yu J, Zhuang A, Gu X, Hua Y, Yang L, Ge S, et al. Nuclear PD-L1 promotes EGR1-mediated angiogenesis and accelerates tumorigenesis. Cell Discov. 2023;9(1):33.
- 32. Pfister SX, Ashworth A. Marked for death: targeting epigenetic changes in cancer. Nat Rev Drug Discov. 2017;16(4):241–63.
- Yuan H, Yan M, Zhang G, Liu W, Deng C, Liao G, et al. CancerSEA: a cancer single-cell state atlas. Nucleic Acids Res. 2019;47(D1):D900-d8.

- Durante MA, Rodriguez DA, Kurtenbach S, Kuznetsov JN, Sanchez MI, Decatur CL, et al. Single-cell analysis reveals new evolutionary complexity in uveal melanoma. Nat Commun. 2020;11(1):496.
- Cho E, Feng Y, Rauskolb C, Maitra S, Fehon R, Irvine KD. Delineation of a Fat tumor suppressor pathway. Nat Genet. 2006;38(10):1142–50.
- Zang ZJ, Cutcutache I, Poon SL, Zhang SL, McPherson JR, Tao J, et al. Exome sequencing of gastric adenocarcinoma identifies recurrent somatic mutations in cell adhesion and chromatin remodeling genes. Nat Genet. 2012;44(5):570–4.
- 37. Berndt A, Cario CL, Silva KA, Kennedy VE, Harrison DE, Paigen B, et al. Identification of fat4 and tsc22d1 as novel candidate genes for spontaneous pulmonary adenomas. Cancer Res. 2011;71(17):5779–91.
- Dhawan A, Scott JG, Harris AL, Buffa FM. Pan-cancer characterisation of microRNA across cancer hallmarks reveals microRNA-mediated downregulation of tumour suppressors. Nat Commun. 2018;9(1):5228.
- 39. Shi H, Wei J, He C. Where, When, and How: Context-Dependent Functions of RNA Methylation Writers, Readers, and Erasers. Mol Cell. 2019;74(4):640–50.
- Jones PA, Issa JP, Baylin S. Targeting the cancer epigenome for therapy. Nat Rev Genet. 2016;17(10):630–41.
- 41. Mohammad HP, Barbash O, Creasy CL. Targeting epigenetic modifications in cancer therapy: erasing the roadmap to cancer. Nat Med. 2019;25(3):403–18.
- 42. Sundaramurthi H, García-Mulero S, Tonelotto V, Slater K, Marcone S, Piulats JM, et al. Uveal Melanoma Cell Line Proliferation Is Inhibited by Ricolinostat, a Histone Deacetylase Inhibitor. Cancers (Basel). 2022;14(3).
- Souri Z, Jochemsen AG, Versluis M, Wierenga APA, Nemati F, van der Velden PA, et al. HDAC Inhibition Increases HLA Class I Expression in Uveal Melanoma. Cancers (Basel). 2020;12(12).
- Li Z, Peng Y, Li J, Chen Z, Chen F, Tu J, et al. N(6)methyladenosine regulates glycolysis of cancer cells through PDK4. Nat Commun. 2020;11(1):2578.
- 45. Yin H, Chen L, Piao S, Wang Y, Li Z, Lin Y, et al. M6A RNA methylation-mediated RMRP stability renders proliferation and progression of non-small cell lung cancer through regulating TGFBR1/SMAD2/SMAD3 pathway. Cell Death Differ. 2023;30(3):605–17.
- 46. Chen H, Gao S, Liu W, Wong CC, Wu J, Wu J, et al. RNA N(6)-Methyladenosine Methyltransferase METTL3 Facilitates Colorectal Cancer by Activating the m(6)A-GLUT1-mTORC1 Axis and Is a Therapeutic Target. Gastroenterology. 2021;160(4):1284– 300 e16.
- 47. Ma JZ, Yang F, Zhou CC, Liu F, Yuan JH, Wang F, et al. METTL14 suppresses the metastatic potential of hepatocellular carcinoma by modulating N(6) -methyladenosine-dependent primary MicroRNA processing. Hepatology. 2017;65(2):529–43.
- Yang Z, Yang S, Cui YH, Wei J, Shah P, Park G, et al. METTL14 facilitates global genome repair and suppresses skin tumorigenesis. Proc Natl Acad Sci U S A. 2021;118(35):e2025948118.
- Liu J, Eckert MA, Harada BT, Liu SM, Lu Z, Yu K, et al. m(6)A mRNA methylation regulates AKT activity to promote the proliferation and tumorigenicity of endometrial cancer. Nat Cell Biol. 2018;20(9):1074–83.

- Liu J, Gu J, Feng Z, Yang Y, Zhu N, Lu W, et al. Both HDAC5 and HDAC6 are required for the proliferation and metastasis of melanoma cells. J Transl Med. 2016;14:7.
- 51. Fiziev P, Akdemir KC, Miller JP, Keung EZ, Samant NS, Sharma S, et al. Systematic Epigenomic Analysis Reveals Chromatin States Associated with Melanoma Progression. Cell Rep. 2017;19(4):875–89.
- Wang L, Leite de Oliveira R, Huijberts S, Bosdriesz E, Pencheva N, Brunen D, et al. An Acquired Vulnerability of Drug-Resistant Melanoma with Therapeutic Potential. Cell. 2018;173(6):1413– 25.e14.
- 53. Balliu M, Guandalini L, Romanelli MN, D'Amico M, Paoletti F. HDAC-inhibitor (S)-8 disrupts HDAC6-PP1 complex prompting A375 melanoma cell growth arrest and apoptosis. J Cell Mol Med. 2015;19(1):143–54.
- 54. Wang W, Huang Q, Chen Y, Huang Z, Huang Y, Wang Y, et al. The novel FAT4 activator jujuboside A suppresses NSCLC tumorigenesis by activating HIPPO signaling and inhibiting YAP nuclear translocation. Pharmacol Res. 2021;170:105723.
- 55. Zhao X, Yang Y, Sun BF, Shi Y, Yang X, Xiao W, et al. FTO-dependent demethylation of N6-methyladenosine regulates mRNA splicing and is required for adipogenesis. Cell Res. 2014;24(12):1403–19.
- Wang X, Zhao BS, Roundtree IA, Lu Z, Han D, Ma H, et al. N(6)-methyladenosine Modulates Messenger RNA Translation Efficiency. Cell. 2015;161(6):1388–99.

- 57. Wei R, Xiao Y, Song Y, Yuan H, Luo J, Xu W. FAT4 regulates the EMT and autophagy in colorectal cancer cells in part via the PI3K-AKT signaling axis. J Exp Clin Cancer Res. 2019;38(1):112.
- 58. Cai J, Feng D, Hu L, Chen H, Yang G, Cai Q, et al. FAT4 functions as a tumour suppressor in gastric cancer by modulating Wnt/beta-catenin signalling. Br J Cancer. 2015;113(12):1720–9.
- Gao YB, Chen ZL, Li JG, Hu XD, Shi XJ, Sun ZM, et al. Genetic landscape of esophageal squamous cell carcinoma. Nat Genet. 2014;46(10):1097–102.

SUPPORTING INFORMATION

Additional supporting information can be found online in the Supporting Information section at the end of this article.

How to cite this article: Zhuang A, Gu X, Ge T, Wang S, Ge S, Chai P, et al. Targeting histone deacetylase suppresses tumor growth through eliciting METTL14-modified m⁶A RNA methylation in ocular melanoma. Cancer Commun. 2023;43:1185–1206.

https://doi.org/10.1002/cac2.12471